nature portfolio

https://doi.org/10.1038/s41551-021-00685-1

Supplementary information

An epidermal patch for the simultaneous monitoring of haemodynamic and metabolic biomarkers

In the format provided by the authors and unedited

Contents

List of Abbreviations

AA	Ascorbic acid
AC	acetaminophen
AL	Alcohol
AOx	Alcohol oxidase
BAC	Blood alcohol concentration
BP	Blood pressure
CA	Chronoamperometry
CF	Caffeine
DPV	Differential pulse voltammetry
ECG	Electrocardiogram
EEG	Electroencephalogram
EKG	Electrocardiogram
EMF	Electromotive force
GLU	Glucose
GOx	Glucose oxidase
HR	Heart rate
IP	Iontophoresis
ISF	Interstitial fluid
LA	Lactate
LOx	Lactate oxidase
NO	Nitric oxide
PB	Prussian blue
PZT	Piezoelectric lead zirconate titanate
RPM	Rotations per minute
SEBS	Styrene-ethylene-butylene-styrene block copolymer
SEM	Scanning electron microscope
UA	Uric acid
US	Ultrasound

Supplementary Note 1. Sensor Fabrication Protocols:

Fabrication of the SEBS substrate. A viscus SEBS resin was prepared by dispersing SEBS beads in toluene with a weight ratio of 1: 2. The mixture was left on a linear shaker (Scilogex, SK-L180-E) overnight or until the mixture became transparent and homogeneous. A PET film with non-stick coating was used as the temporary casting substrate, and a doctor blade set at 1 mm height was used to cast the SEBS resin into a sheet on the PET substrate. The cast resin was firstly dried in ambient environment for 1 h, followed by curing in a conventional oven at 80 °C for additional 1 h to remove the excess solvent. The transparent, uniform SEBS film was peeled off from the PET substrate for subsequent sensor fabrication.

Synthesis of the stretchable silver and PB ink. The formulation of the stretchable silver ink is based on early reports.[1] The ink was synthesized by mixing silver flakes, toluene, and SEBS, in a weight ratio of 4: 2.37: 0.63, in a dual asymmetric centrifugal mixer (Flacktek Speedmixer, DAC 150.1 KV-K) with a speed of 1800 RPM for 10 min or until obtaining a homogeneous ink. The stretchable PB ink was synthesized by mixing super-P carbon black, graphite powder, PB, SEBS and toluene, in a weight ratio of 0.5: 3: 1: 1.26: 4.74, in the mixer at 2150 RPM for 10 min or until the ink was homogeneous. Before printing the stretchable inks, the ink viscosity was analyzed visually and, if necessary, (~200 µL) toluene was added and the ink was centrifuged before use.

Printing of the stretchable electrodes. The prepared SEBS sheet was used as the stretchable substrate for the printed electrodes. Firstly, stretchable silver ink was used for printing the interconnections, the IP electrodes, and the reference electrodes, on the front part of the SEBS substrate. Next, the stretchable PB ink was used to print the working and counter electrodes of the biosensors. The SEBS substrate was then turned over and the interconnections for the transducer array were printed on the backside of the SEBS substrate (opposite to the printed PB ink), with one extra channel reserved for connecting to the common ground of the transducers. A separate piece of SEBS sheet was used to print the ground wire for the transducers. The printed inks were cured in a conventional oven at 80 °C for 10 min after each printing step. The step-by-step printing of the electrode is illustrated in **Supplementary Figure 1**. Before using the complete printed device, the stretchable silver reference electrodes were treated by adding a droplet (10 µL) of 0.1 M $FeCl_3$ in 0.1 M KCl on the printed surface for 20 seconds to produce the Ag/AgCl layer.

Assembly of the PZT transducers. The diced PZT transducers can be "solvent soldered" onto the printed current collectors by firstly dissolving the junction regions of the interconnections temporarily with a small volume of toluene (~ 1µL), followed by placing the transducers onto the softened trances to physically bond with the composite ink. After placing the transducers onto the wetted interconnections, the assembled device was left drying for 2 minutes in ambient temperature. Afterward, the printed ground wire was carefully aligned with the transducers and solvent soldered to the array, by adding a droplet of toluene on each PZT transducer, in a similar fashion. Lastly, the printed ground was "solvent soldered" to the reserved channel of the interconnection array. The detailed fabrication process is illustrated in **Supplementary Figure 2**.

Biosensor Working electrode modification. All PBS used in the electrode modification was prepared in 0.1 M with a pH of 7.4. All BSA solution was prepared with a concentration of 10 mg/mL in PBS. The chitosan solution was prepared by dissolving chitosan in 0.1 M acetic acid with a concentration of 0.5 wt%. For preparing the lactate biosensor, the chitosan solution was mixed with LOx (40 mg/mL) in BSA solution, in a ratio of 1: 1 (v/v), followed by drop casting a 2 µL aliquot of the mixture onto the working electrode surface. For preparing the glucose biosensor, GOx (40 mg/mL) in BSA solution, glutaraldehyde in water (5 wt%) and Nafion in water (0.5 wt%) were mixed in a ratio of 1: 1: 0.33 (v/v/v) , and a 1.5 µL aliquot was drop cast onto the working electrode surface. For preparing the alcohol biosensor, AOx (10-40 units/mg), BSA solution and the chitosan solution were mixed in a ratio of 8:1:1 (v/v/v), and a 4 µL aliquot of the mixture was drop cast to the working electrode surface. After drying at room temperature for 1 hr, 2 µL of the chitosan solution was drop cast to all previously enzyme-modified surfaces. Upon completing the corresponding modification steps, the resulting biosensors were stored at 4°C overnight before using. For the caffeine sensor, a solution of 0.1 mg/mL of MWCNT was dispersed in 50% EtOH (v/v in DI water) in an ultrasound bath for 10 min, and a 2 µL aliquot of the dispersed solution was drop cast onto the working electrode surface. After drying at room temperature for 1 hr, 2 µL of 0.01% v/v of Nafion in water solution was drop cast onto the previously MWCNT-decorated working electrode and dried at room temperature overnight. Schematics representing the modified sensor components and corresponding electrochemical reactions are shown in **Supplementary Figure 5.**

Preparation of the IP hydrogels. An Ecoflex mold with multiple circular trenches with a diameter of 18 mm and thickness of at least 1 mm was prepared for forming the hydrogels. The anode hydrogel solution was prepared by dissolving 120 mg agarose in 3 mL of 0.1 M phosphate-buffered saline solution at 150 °C under stirring until all agarose was dissolved. The cathode hydrogel solution was prepared by dissolving 120 mg agarose in 3 mL DI water. After agarose dissolution, the temperature was immediately decreased to 60 ºC and 60 mg of pilocarpine was added under continuous stirring. 300 µL aliquots of the hot solutions (cathodic and anodic gels) were added into each circular mold to allow them to solidify. After the solution cooled down in the mold, the gels were cut into the corresponding cathode and anode geometries and stored in a wet chamber at 4 °C before using. The detailed preparation procedure is illustrated in **Supplementary Figure 21.**

Supplementary Note 2. Sensor in-vitro characterization

All PBS used in the in-vitro characterization of the sensors is 0.1 M at pH 7.4, unless otherwise noted.

Lactate sensor. The calibration curve of the lactate sensor was obtained using an initial PBS droplet with 100 µL volume on the sensor surface. The solution was spiked with 1 µL of 0.5 M lactate solution to incrementally increase the concentration of the lactate from 0 to 30 mM with CA at -0.2 V for 60 s after each spiking. The selectivity of the lactate sensor was evaluated by performing CA while spiking the PBS successively with lactate (2 mM), glucose (0.2 mM), ascorbic acid (10 µM), uric acid (60 µM), and acetaminophen (10 µM).[2] The stability of the lactate sensor was examined by performing 10 repetitive CA measurements of 2 mM lactate and calculating its relative response changes in %. The in-vitro characterization data of the lactate sensor is summarized in **Supplementary Figure 6**.

Glucose sensor. The calibration curve of the glucose sensor was obtained using an initial 100 µL PBS droplet on the sensor surface The solution was spiked with 1 µL of 0.1 M glucose solution to incrementally increase the concentration of glucose from 0 to 10 mM with CA at -0.2 V for 60 s after each spiking. The selectivity of the glucose sensor was evaluated by performing CA while spiking the PBS successively with glucose (2 mM), lactate (10 mM), ascorbic acid (10 µM), uric acid (10 µM), and acetaminophen (10 µM).[2] The stability of the glucose sensor was examined by performing 10 repetitive CA measurements of 2 mM glucose and calculating its relative response changes in %. The in-vitro characterization data of the glucose sensor is summarized in **Supplementary Figure 7**.

Alcohol sensor. The calibration curve of the alcohol sensor was obtained using an initial PBS droplet with 100 µL volume on the sensor surface. The solution was spiked with 1 µL of 0.8 M ethanol solution to incrementally increase the concentration of alcohol from 0 to 32 mM with CA at -0.2 V for 60 s after each spiking. The selectivity of the alcohol sensor was evaluated by performing CA while spiking the PBS measured successively with ethanol (20 mM), lactate (10 mM), glucose, (0.2 mM), ascorbic acid (10 µM), uric acid (60 µM), and acetaminophen (10 µM).[2] The stability of the alcohol sensor was evaluated by performing 10 repetitive CA measurements of 2 mM ethanol and calculating its relative response changes in %. The in-vitro characterization data of the alcohol sensor is summarized in **Supplementary Figure 8**.

Caffeine sensor. DPV was utilized for evaluating the caffeine sensor with the following parameters: accumulation at -1.2 V for 30s; $E_{initial}$: +0.5 V; E_{final}: +1.5 V; E_{step}: 0.004 V; E_{pulse}: 0.05 V; t_{pulse}: 0.05 s; scan rate: 0.02 V/s. For calibration curve tests, 100 µL of 0.01 M acetate buffer (pH 4.5) were used to cover the sensing area of the device. The background response was recorded repeatedly until the signal was stable. The caffeine DPV response was then recorded after each consecutive addition of 1 µL of 1 mM caffeine in DI water for obtaining 10 µM increments of the caffeine concentration, up to 210 µM. The selectivity of the caffeine sensor was evaluated by performing DPV while spiking the acetate buffer successively with caffeine (20 µM), lactate (10 mM), ascorbic acid (10 µM), uric acid (60 µM), and acetaminophen (10 µM).[2] The stability of the caffeine sensor was examined by performing 10 repetitive DPV measurements of 20 µM caffeine and calculating its relative peak current changes in %. The in-vitro characterization data of the caffeine sensor is summarized in **Supplementary Figure 9**. For the on-body tests an agarose gel loaded with acetate buffer pH 4.5 was used, covering only the caffeine sensor. A standard additions voltammetric method, involving spiking caffeine to a collected sweat sample, is used to validate the amount of caffeine in sweat. This method was used once to construct the calibration plot for correlating directly the wearable patch signal to sweat caffeine concentrations.

Sodium sensor. Open circuit potential (OCP) was used for evaluating the sodium sensor. For the calibration curve, the sensor was incubated for 30 minutes in an aqueous solution of 10 mM NaCl. After rinsing, the response signals for 100 µL of 0.1, 1, 10 and 100 mM NaCl were recorded by consecutively replacing the solution on the electrode surface. The selectivity of the sodium sensor was evaluated by calibrating the sensor with different KCl concentrations in a similar fashion as the NaCl calibration. The stability of the sodium sensor was examined by recording the response to 0.1 mM NaCl over 1 hour. The reversibility of the sensor was performed by increasing and decreasing the NaCl concentration on the sensor surface from 0.1 mM to 100 mM and back to 0.1 mM.

Supplementary Note 3. Calibration of blood pressure waveform:

The position of the artery walls was represented by the flight time of the echo signals. By continuously tracking the echo shift of the vessel walls, the arterial distension waveform could be recorded (**Supplementary Figure 10**).[3] Then, based on an established model[4], the arterial distension waveform could be transferred to blood pressure waveforms[3].

The arterial blood pressure waveform $p(t)$ is calculated from the vessel distension waveform $d(t)$ as follows:

$$A(t) = \frac{\pi d^2(t)}{4}$$

$$p(t) = p_d \cdot e^{\alpha(\frac{A(t)}{A_d}-1)}$$

where $A(t)$ is the cross-sectional area of the artery, and $d(t)$ is the diameter of the target artery. Here, the artery is assumed to be rotationally symmetrical. p_d is the diastolic pressure. A_d is the diastolic arterial cross-section, and α is the rigidity coefficient.

α can be calculated by following equation:

$$\alpha = \frac{A_d \ln(p_s / p_d)}{A_s - A_d}$$

where A_s is the systolic arterial cross-section, and p_s is the systolic pressure. The p_d and p_s are measured by the commercial blood pressure cuff from the brachial site. Using the above equations and a brief calibration for *α*, p_d, and p_s the accurate pressure waveform $p(t)$ can be obtained.

It is worth noting that we assume that the human blood vessel is elastic with negligible viscoelasticity. For subjects with normal local vascular conditions or with slight local atherosclerosis, the diameter of the vessel does not lag behind the pressure waveforms [4,5]

Supplementary Note 4. Simultaneous Monitoring of ISF and Sweat analytes via Iontophoresis

An iontophoretic system has been used for the simultaneous ISF extraction (cathode) and sweat stimulation by pilocarpine delivery (anode). The extraction and delivery operations are performed at the same time based on two mechanisms, as described in detail in previously published work[2]. In summary, a low-intensity electrical current is applied to the skin using two electrodes (cathode and anode). Iontophoretic gels with different compositions are located under each electrode. On the anode compartment, a pilocarpine-loaded gel is used for stimulating the sweat. Pilocarpine is delivered inside the skin by electrical repulsion as the pilocarpine molecule is positively charged and a positive current is applied at the anode. Then, localized sweat production occurs only in the stimulated area where the pilocarpine drug was delivered (anode). Since no sweat stimulant drug is present on the cathode compartment, no sweat is produced under the cathode electrode. The iontophoretic gel, located in the cathode compartment, is loaded with PBS buffer and a negatively charged current is applied to attract the positively charged ions from the ISF under the skin to the outside. A flow of negatively-charged ions is also attracted to the skin surface in the anode compartment; however, as the skin is naturally negatively charged, there is a net flow of ISF toward the cathode, which carries all small neutral molecules in the same direction. ISF glucose can thus be detected in the cathodic compartment. Accordingly, the electroosmotic convective flow is responsible for the ISF glucose extraction exclusively on the cathode compartment while the target sweat analyte is detected at the anode.

Supplementary Note 5. SEM analysis from Mechanical Deformation

For examining the morphological change of the printed composite electrode before and after stretching, we have prepared 2 sets of samples for the SEM imaging, before and after the 1500 times of stretching. The change in the apparent surface morphology can be caused by several factors, including the difference in the individual samples, the contrast, and brightness of the SEM image being taken, as well as the most importantly, any physical damage caused by the stretching deformation. The key element we were trying to examine was to identify any, such as cracking, peeling, or delamination, on the surface of the electrode. As we can see from the images provided in the **Supplementary Figure 13 b-c**, the printed silver composite, mainly used as the reference electrode and the interconnection for the electrochemical sensors and the PZT chips, has no apparent cracking, peeling, or delamination from the substrate. The Prussian blue-carbon ink, used for the working and auxiliary electrodes of the electrochemical sensors, has shown minor cracking on the surface of the electrode. Such behavior is expected as the formulation of the carbon-PB ink includes a high loading of small-size, highly porous materials, which made the composite less stretchable compared to the silver-based ink. However, due to the small size and high active surface area of the working electrode, such minor morphological change should have a negligible effect on the sensing results and upon the sensitivity. To support this argument, we have demonstrated the chronoamperometric data in **Figure 2g-l**, which shows that the current response of the electrochemical sensor is not affected by the repeated stretching. Thus, we can conclude that the electrochemical performance of the sensor was not impaired by the mechanical deformation. The acoustic transducers, based solely on the silver ink, rely mainly on the temporal resolution of the signals instead of its intensity, and was also not affected by the stretching deformation. Furthermore, we performed additional mechanical tests to measure the sensor performance during deformation (**Supplementary Figure 15-16**). The results also indicate no hysteresis due to the applied strain on the printed electrodes. We can thus more confidently claim that the sensor should perform normally within the designed level of deformation. As a wearable epidermal sensor, we are assuming the usage of the sensor to be limited to a week; the tested 1000 times of repeated deformation at the strain of 20% to be extreme are unlikely to occur in real life. Compared to bending and twisting, stretching deformation applies the most mechanical stress to the printed materials. Due to the use of hydrogels, abrasion on the electrode is also less likely to occur. The repeated stretching tests were thus used as the most rigorous test for the durability of the sensor. Overall, we believe that the aforementioned supporting data reflect the stable and durable performance of the integrated sensor.

Supplementary Note 6. Sodium Ion Selective Electrode

The sodium selective membrane cocktail composition consisted of 1 mg sodium ionophore X, 0.55 mg Na-TFPB, 33 mg PVC, and 65.45 mg DOS dissolved in 660 µL of THF (Fisher Chemical). The cocktail was

thoroughly mixed to dissolve all the components. The reference cocktail was prepared by dissolving 78.1 mg PVB (Quimidroga S.A.) and 50 mg NaCl in 1 mL methanol. Next, a 3 µL aliquot of the sodium selective membrane cocktail was drop-casted onto the working carbon electrode and the reference electrode was modified by 3 µL aliquot of the reference cocktail, followed by 1 µL of polyurethane (Tecoflex® SG-80A) dissolved in THF (15%w/w). The modified Na-sensors were left to dry overnight before use. All chemicals were obtained from Sigma Aldrich (St. Louis, MO), except when specified otherwise.

Supplementary References

1. Yin, L. *et al.* From All-Printed 2D Patterns to Free-Standing 3D Structures: Controlled Buckling and Selective Bonding. *Adv. Mater. Technol.* **3**, 1800013 (2018).
2. Kim, J. *et al.* Simultaneous Monitoring of Sweat and Interstitial Fluid Using a Single Wearable Biosensor Platform. *Adv. Sci.* (2018). doi:DOI: 10.1002/advs.201800880
3. Wang, C. *et al.* Monitoring of the central blood pressure waveform via a conformal ultrasonic device. *Nat. Biomed. Eng.* **2**, 687–695 (2018).
4. Arndt, J. O., Klauske, J. & Mersch, F. The diameter of the intact carotid artery in man and its change with pulse pressure. *Pflugers Arch. Gesamte Physiol. Menschen Tiere* **301**, 230–240 (1968).
5. Valdez-Jasso, D. *et al.* Linear and nonlinear viscoelastic modeling of aorta and carotid pressure-area dynamics under in vivo and ex vivo conditions. *Ann. Biomed. Eng.* (2011). doi:10.1007/s10439-010-0236-7

Supplementary Figures

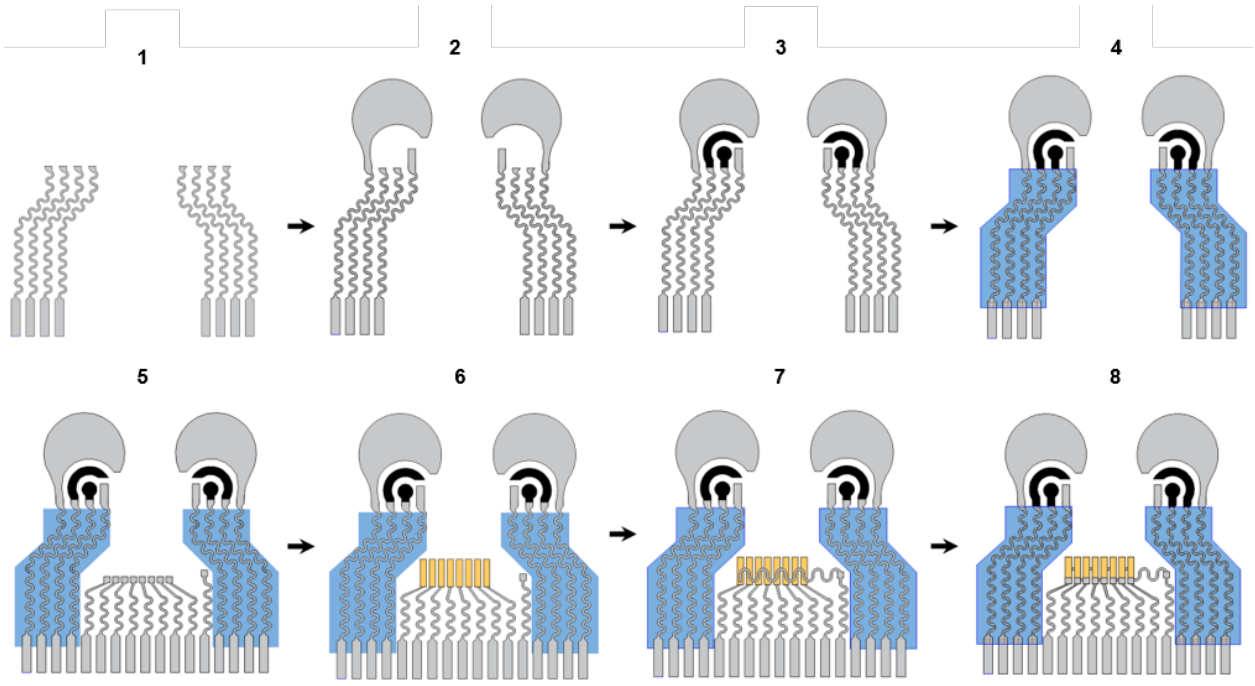

Supplementary Figure 1. Layer-by-layer printing and assembling steps of the integrated sensor. Stretchable silver and PB ink were used to print the pattern over the SEBS substrate. Step 1: Printing the stretchable serpentine interconnection using the silver ink. Step 2: Printing of the IP electrodes and the reference electrodes using the silver ink. Step 3: Printing the the counter (curved) and working electrodes (round) using the PB ink. Step 4: Printing an insulating layer to define the working electrode area and insulate the interconnections using the SEBS resin. Step 5: Flip the SEBS substrate backside up. Print the serpentine interconnects for the transducers and ground using the silver ink. Step 6: Solvent solder the transducer chips onto the silver interconnects. Step 7: Solvent solder the ground to the other side of the transducers and connect it to the reserved ground interconnect. Step 8: Finished. Ready for sensor modifications.

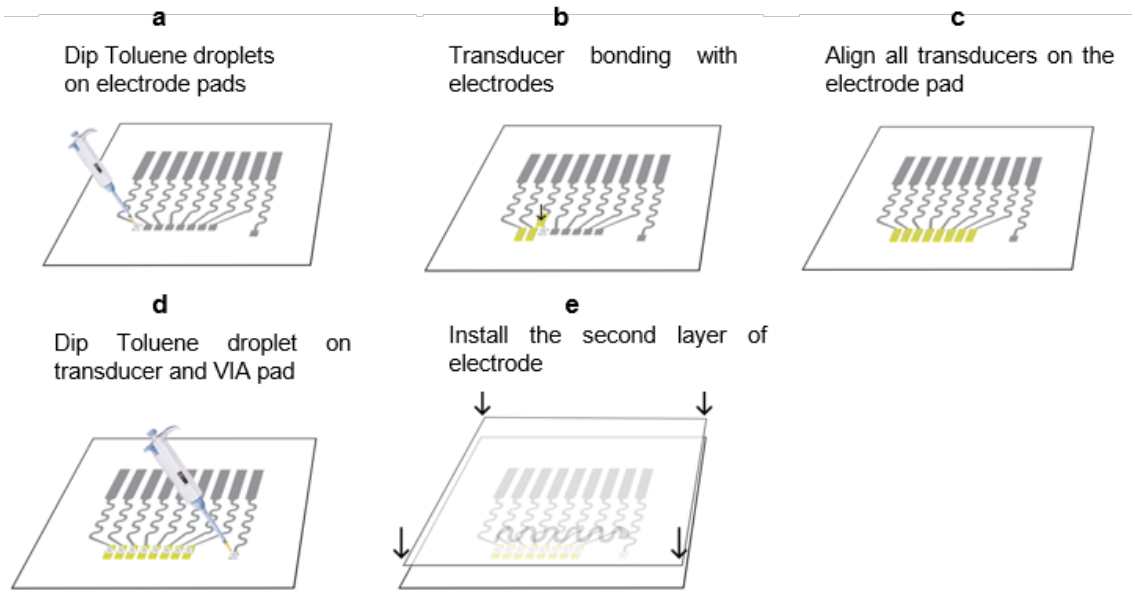

Supplementary Figure 2. Assembly process of ultrasound transducers. **a**, Dip toluene droplets on the connection pad of the interconnects using a pipette to partially dissolve the silver traces. **b**, Place the transducer on the softened pad for bonding. **c**, Repeat steps in **a**-**b** and align all the transducers along the pattern. **d**, Dip toluene droplets on transducers and the ground interconnect pad using a pipette. **e**, Apply the ground wire to the transducers and connect to the ground interconnect pad.

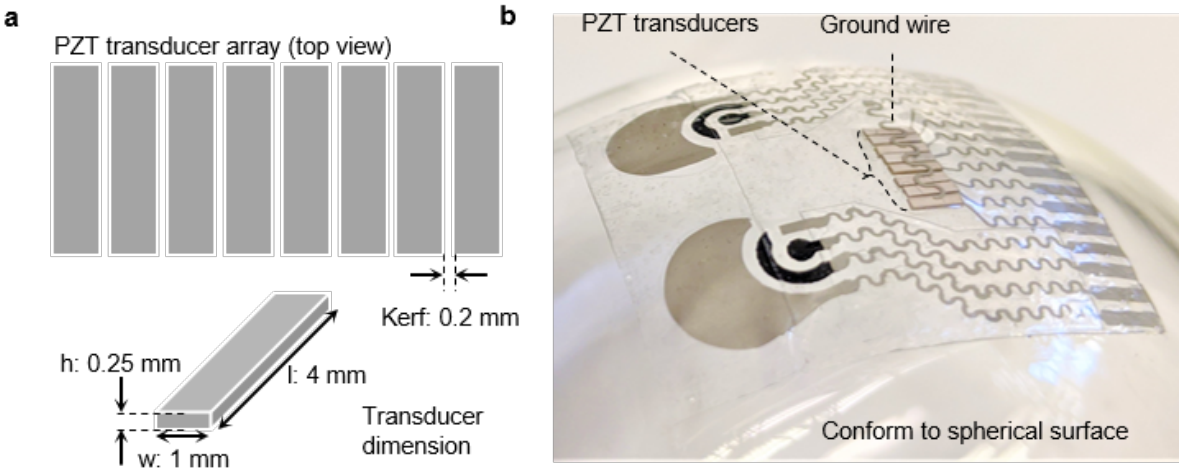

Supplementary Figure 3. Transducer dimensions and conformability. **a**, Dimensions of the PZT transducer pixel and the transducer array. The aspect ratio of each pixel is controlled to be smaller than 0.3 (w, l > 3h) to ensure that the PZT vibration is in thickness mode with accurate frequency (7 MHz). **b**, Photo of the device on a spherical surface to demonstrate the conformability of the fabricated transducer array.

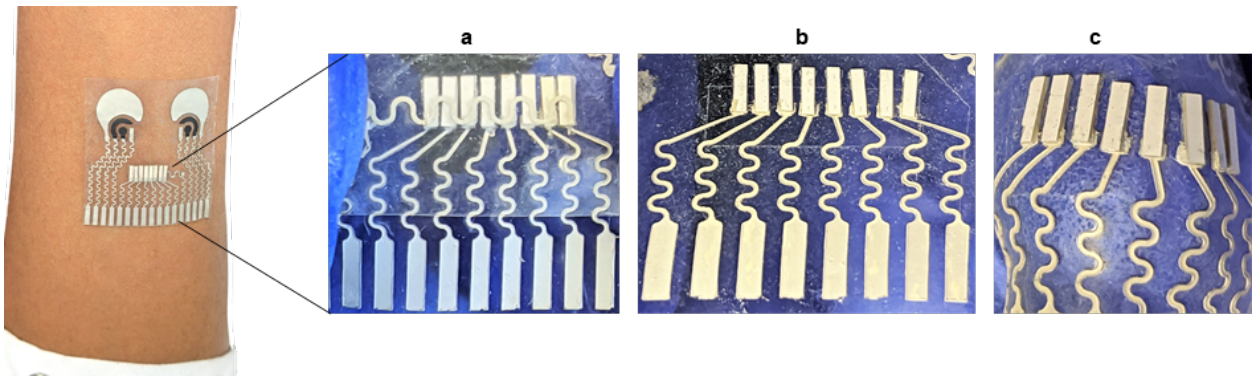

Supplementary Figure 4. Adhesion of the PZT transducers to the substrate. **a**-**c**, The photo images of the pristine device before any deformation (**a**), the device during horizontal stretching (**b**) and under indentation (**c**). The PZT transducers remained well attached to the printed silver traces after the deformations.

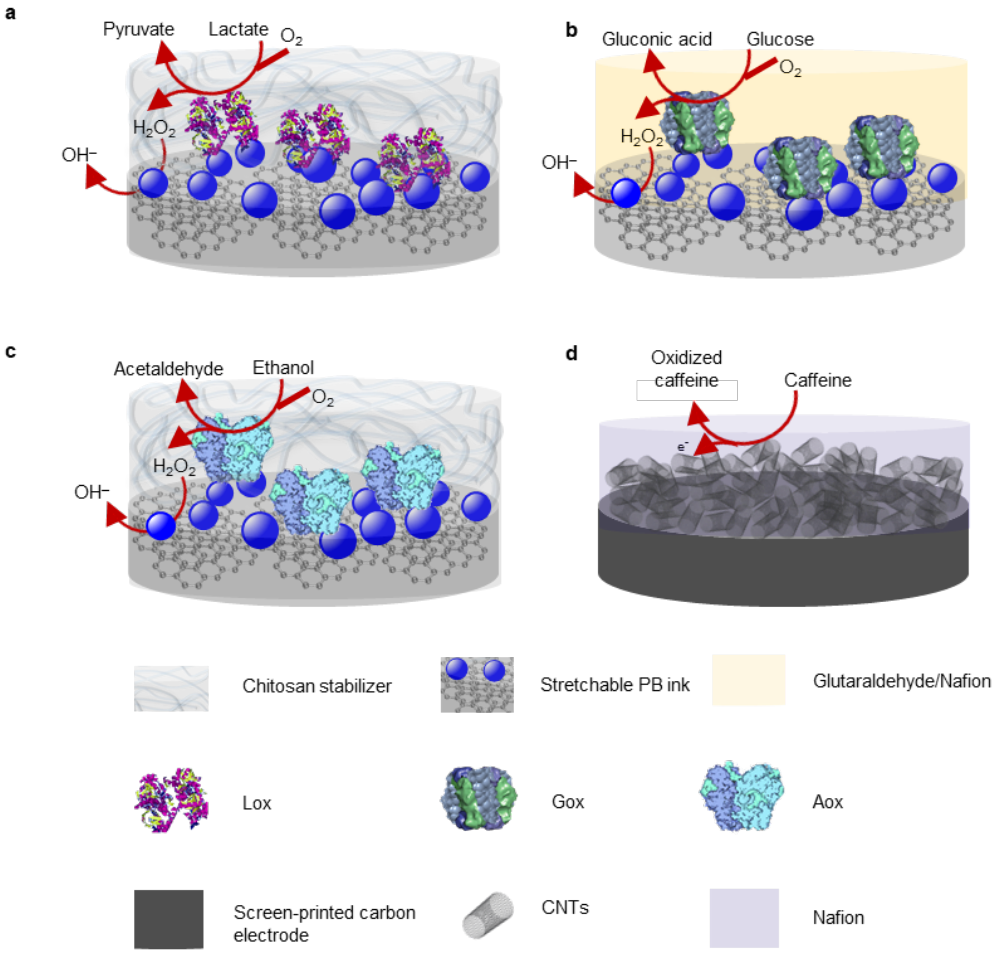

Supplementary Figure 5. Biosensor modifications and reaction mechanisms. a, Lactate sensor modification. LOx reaction with lactate, leading to the formation of hydrogen peroxide and pyruvate. Further, the PB-based electrode transducer transforms the hydrogen peroxide product to hydroxyl ions (OH^-) for selective lactate detection. **b**, Glucose sensor modification. The GOx reaction with glucose leads to the formation of hydrogen peroxide and gluconic acid. The PB based electrode transducer offers specific detection of the peroxide product towards selective glucose detection. **c**, Alcohol sensor modification. The AOx reaction with its ethanol substrate results in the formation of hydrogen peroxide and acetaldehyde. The PB-based electrode transducer offers specific detection of the peroxide product towards selective alcohol detection. **d**, Caffeine sensor modification. The anodic oxidation of the caffeine analyte at the CNT modified printed

electrode results the production of uric acid and electron flow. The DPV peak current corresponds to the caffeine concentrations.

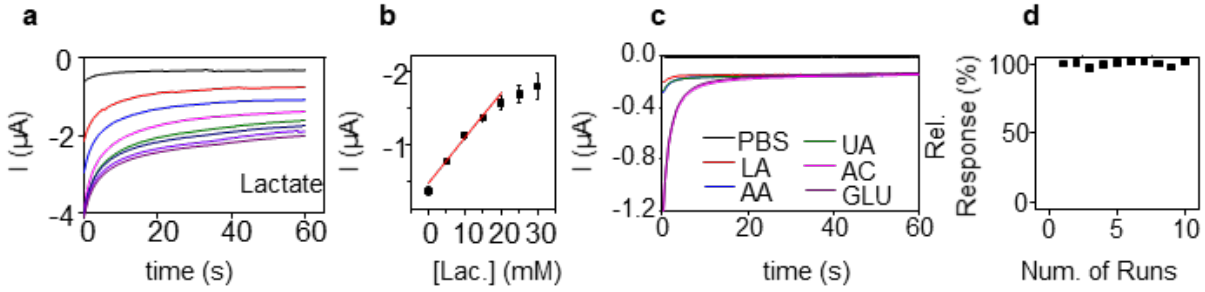

Supplementary Figure 6. In-vitro characterization of the lactate sensor. a, Lactate sensor's amperometric response to successive additions of 5 mM lactate from 0 to 30 mM. **b**, Lactate calibration curve based on the average response of different sensors (RSD = 6%, n=3, r^2= 0.98). **c**, Evaluation of the lactate sensor selectivity in the presence of lactate (LA, 2 mM), glucose (GLU, 0.2 mM), ascorbic acid (AA, 10 μM), uric acid (UA, 60 μM) and acetaminophen (AC, 10 μM). (d) Stability of the lactate: 10 repetitive measurements of 2 mM lactate.

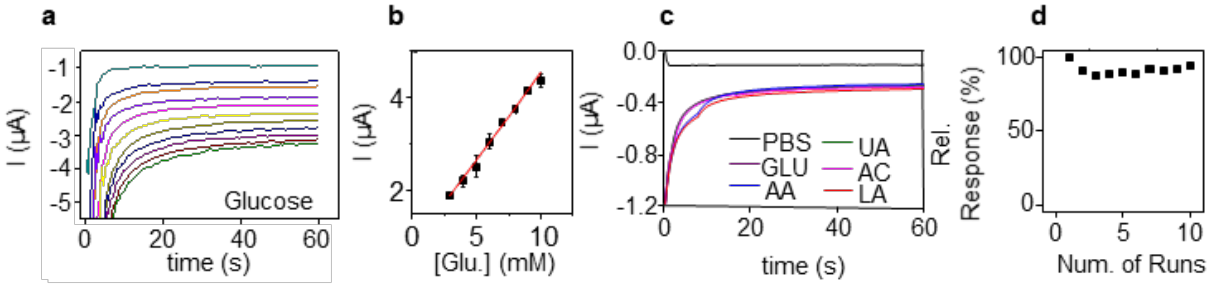

Supplementary Figure 7. In-vitro characterization of the glucose sensor. a, Glucose sensor's amperometric response to successive 1 mM glucose additions from 0 to 10 mM. **b**, Glucose calibration curve based on the average response of different sensors (RSD = 3.6%, n=3, r^2= 0.99), Evaluation of the glucose sensor selectivity in the presence of GLU (2 mM), LA (10 mM), AA (10 μM), UA (10 μM) and AC (10 μM). **d**, Stability of the glucose sensor: 10 repetitive measurements of 2 mM glucose.

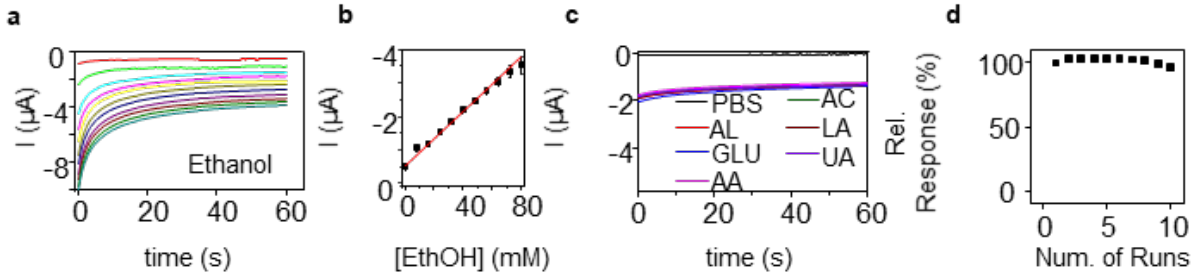

Supplementary Figure 8. In-vitro characterization of the alcohol sensor. **a**, The alcohol sensor's amperometric response to successive 8mM ethanol increments from 0 to 80 mM. **b**, Calibration curve of the alcohol sensor based on the average response of different sensors (RSD = 3.5%, n=3, r^2=0.99). **c**, Selectivity test in the presence of AL (20 mM), GLU (0.2 mM), AA (10 μM), LA (10 mM), UA (60 μM) and AC (10 μM). **d**, Stability of the alcohol sensor: 10 repetitive measurements of 20 mM alcohol.

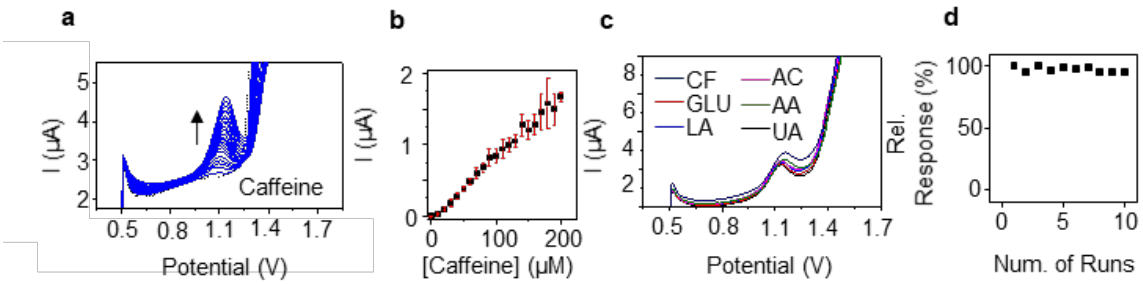

Supplementary Figure 9. In-vitro characterization of the caffeine sensor. a, the caffeine sensor's DPV response of increasing caffeine additions in 10 μM steps from 0 to 200 μM. **b**, Corresponding caffeine calibration curve based on average response of different sensors (RSD = 0.14%, n=3, r^2=0.9). **c**, Evaluation of the caffeine sensor selectivity in the presence of CF (20 μM), GLU (0.2 mM), LA (10 mM), AA (10 μM), UA (60 μM) and AC (10 μM). **d**, Stability of the caffeine sensor: 10 repetitive DPV measurements of 20 μM caffeine.

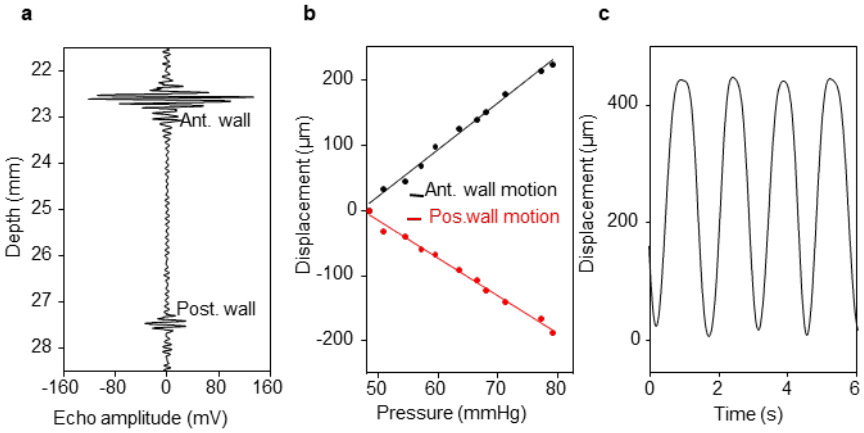

Supplementary Figure 10. Ultrasound transducer characterization on phantom. a, Radio frequency signal showing the anterior wall and posterior wall of the carotid artery phantom. **b**, Vessel wall displacement with increased intravascular pressure on phantom. **c**, Periodic vessel distension induced by the inflator.

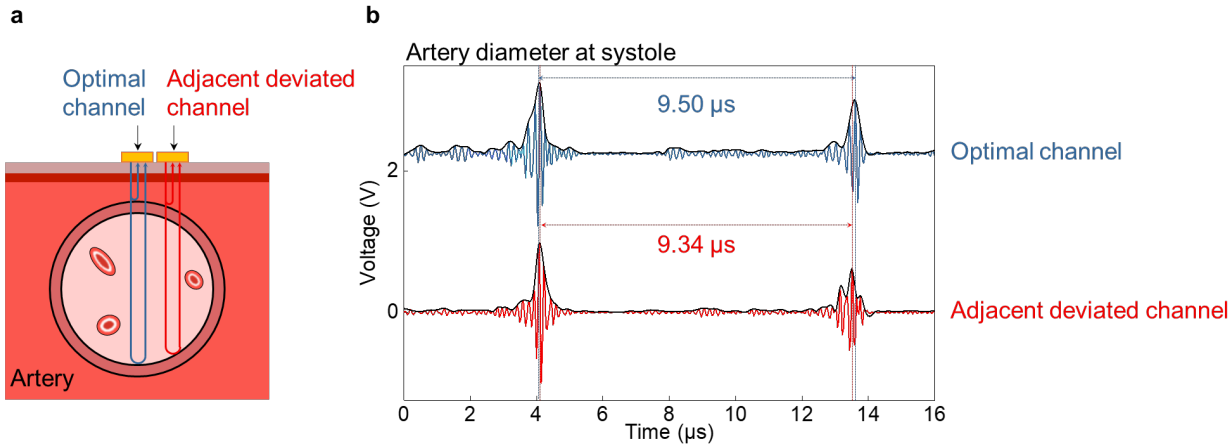

Supplementary Figure 11. Optimal channel selection for accurate artery diameter tracking. a, The optimal channel was determined by calculating the time of flight (ToF) of the ultrasound signal. **b,** Raw RF signal showing different ToF values from two adjacent transducers. Only the maximum ToF between anterior wall and posterior wall would be recognized as the 'diameter' of the artery. Thus, the accurate diameter tracking could be guaranteed by the channel selection.

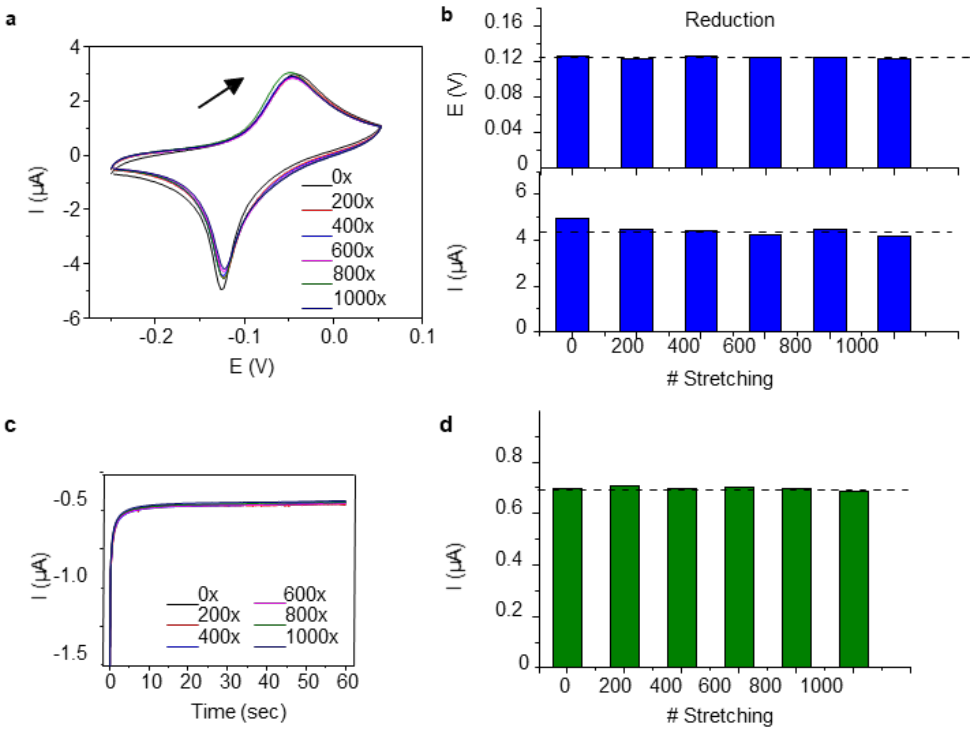

Supplementary Figure 12. Electrode electrochemical stability under repeated stretching tests. **a-b**, the CV response of the PB electrode every 200 cycles in a 1000-cycle, 20% strain stretching test (**a**) and the corresponding reduction peak potentials (RSD = 0.84%) and peak currents (RSD = 5.55%). **c-d**, The CA response at -0.2 V applied anodic potential of the PB electrode every 200 cycles in a 1000-cycle, 20% strain stretching test (**a**), and the corresponding end-point currents (**d**). All electrochemical tests were performed in 0.1M PBS with pH 7.4, against an Ag/AgCl reference electrode.

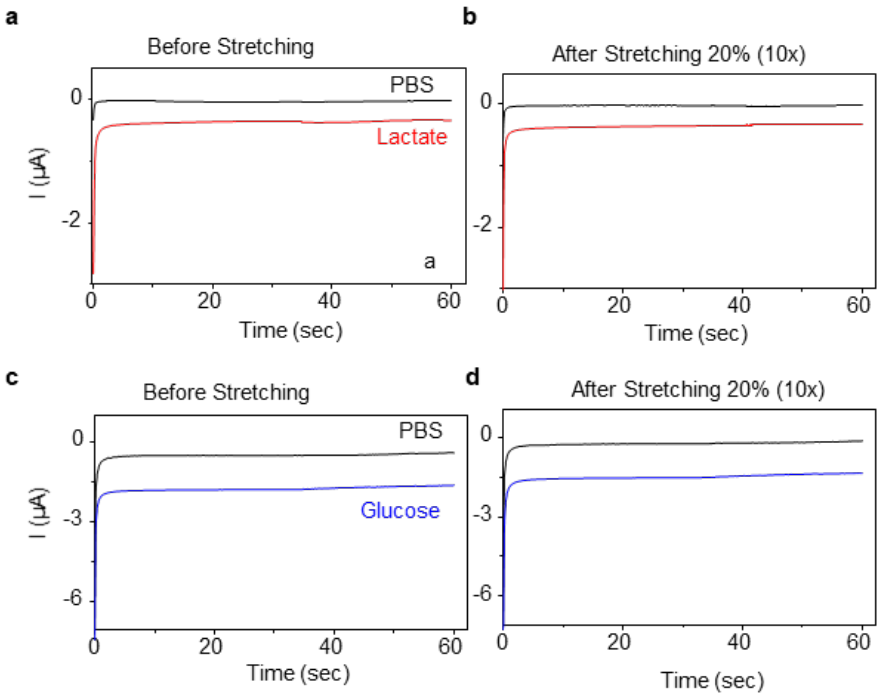

Supplementary Figure 13. Sensor electrochemical stability under repeated stretching tests. a-b, the response of modified lactate sensor to 2 mM lactate before (**a**) and after (**b**) 10 cycles of 20% stretching. **c-d**, the response of modified glucose sensor to 10 mM glucose before (**a**) and after (**b**) 10 cycles of 20% stretching. CA was recorded using a potential of -0.2 V in 0.1 M PBS with pH 7.4.

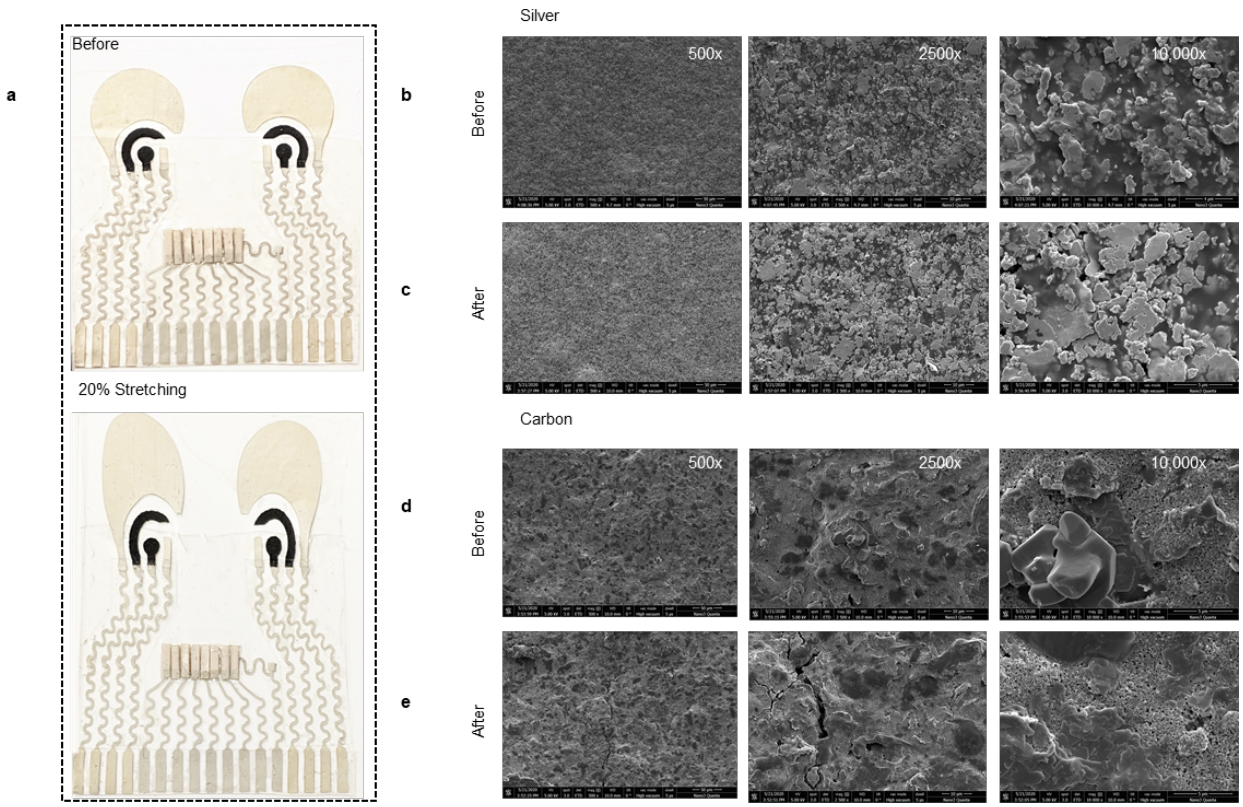

Supplementary Figure 14. Structural integrity of the stretchable silver and PB/carbon ink composites. **a**, Photo illustration of the device before and after stretched to 120%. **b-e**, SEM images in different magnifications of the silver trace before (**b**) and after (**c**) 1000 cycles of 20% stretching, and of the carbon trace before (**d**) and after (**e**) 1000 cycles of 20% stretching.

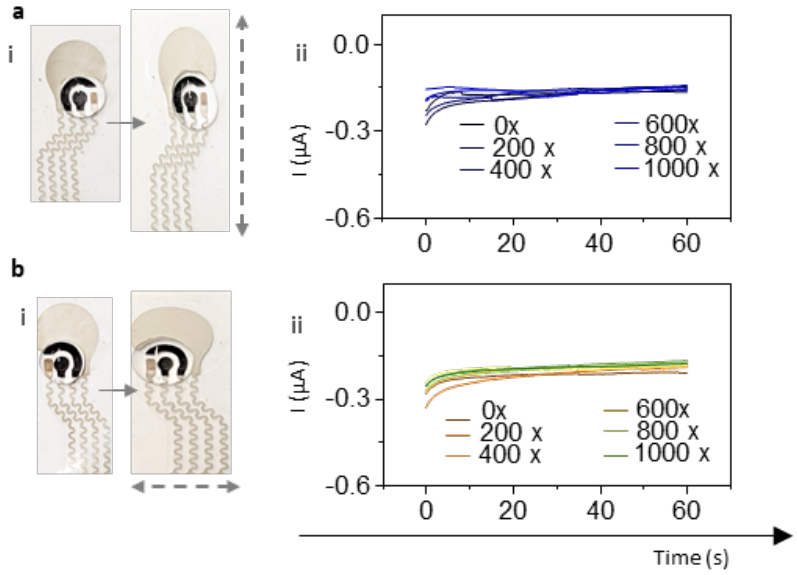

Supplementary Figure 15. Electrochemical performance under mechanical deformation. a, Photo of the sensor under 20% vertical strain (i), and electrochemical response (chronoamperometry at -0.2V in PBS 0.1M, pH 7) under 20% stretching every 200 stretching cycles until 1000 cycles (RSD = 18.6%). **b,** Photo of the sensor under 20% horizontal strain (i), and electrochemical response (chronoamperometry at -0.2V in PBS 0.1M, pH 7 under 20% stretching every 200 stretching cycles until 1000x (RSD = 15.8%).

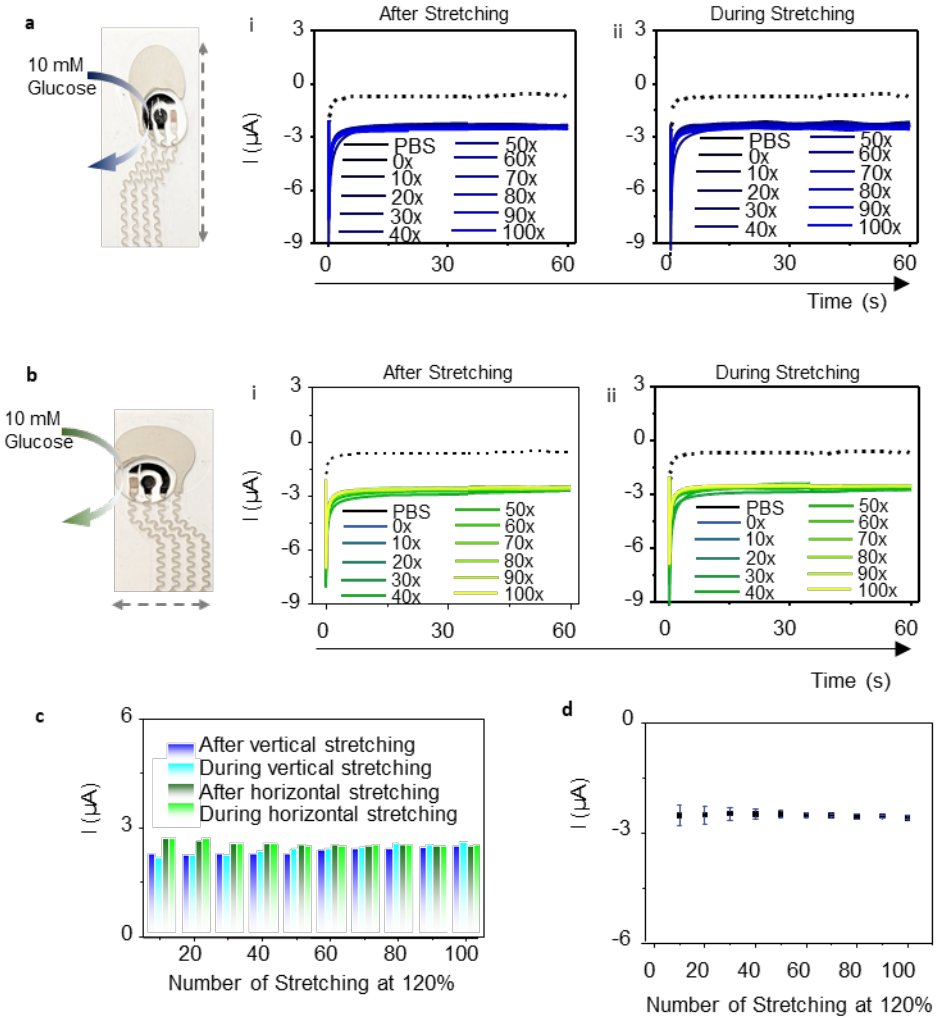

Supplementary Figure 16. Electrochemical performance of the GOx modified biosensor under mechanical deformation. a, Photo of the sensor under 20% vertical strain and electrochemical response to 10 mM glucose after stretching the sensor vertically 100 times at 120% and recording the signal every 10 stretching cycles (RSD = 3.45%) (i). The response was also recorded while the sensor was under stress, after every 10-stretching deformation (RSD = 5.42%). **b,** Photo of the sensor under 20% horizontal strain and electrochemical response to 10 mM glucose after stretching the sensor horizontally 100 times at 120% and recording the signal every 10 stretching cycles (RSD = 2.33%) (i). The response was also recorded with the sensor under stress after every 10- stretching deformation (RSD = 3.14%). **c**, Variation of current response to 10 mM glucose for all deformations (RSD = 5.18%). **d**, Error associated to each deformation cycle including all deformations; higher error is associated to the first cycles.

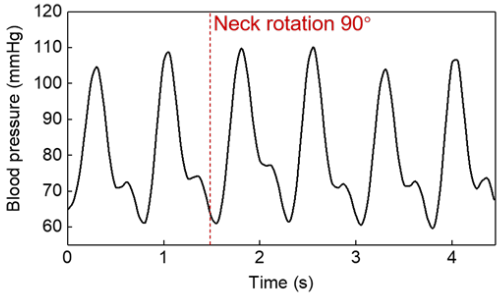

Supplementary Figure 17. The BP signal measured on-body while turning the neck 90° to the side, with no obvious change of signal quality.

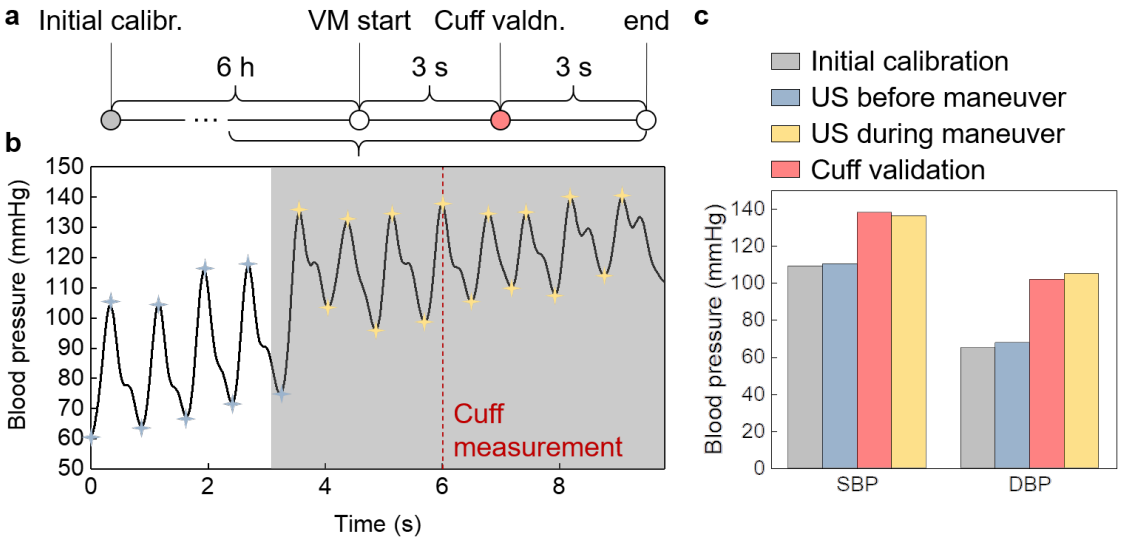

Supplementary Figure 18. The BP variation during the Valsalva maneuver. a, The event timeline of the BP signal recording during a Valsalva maneuver. **b,** The BP waveform during the initial phase of the Valsalva maneuver. A sudden increase in BP is observed. The local peaks (systolic BP) and troughs (diastolic BP) were indicated (blue points – before maneuver, yellow points – during maneuver) **c,** Comparison of the systolic and diastolic BP to the initial cuff calibration, the average BP before and during the maneuver measured by the patch, and the validation using the cuff during the maneuver.

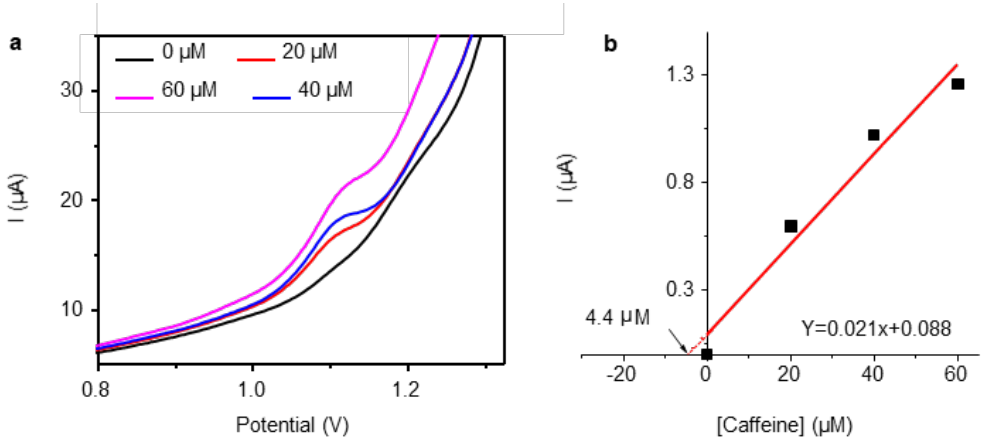

Supplementary Figure 19. Standard additions to determine caffeine concentration in sweat. a, DPV of caffeine in collected sweat (after drinking 114 mg caffeine). Increasing concentrations of caffeine were added to the collected sweat and the respective calibration curve was used to analyze the initial caffeine concentration in sweat **b,** Calibration curve. The horizontal axis shows the concentration range used in the test. The vertical axis shows the current change after each addition.

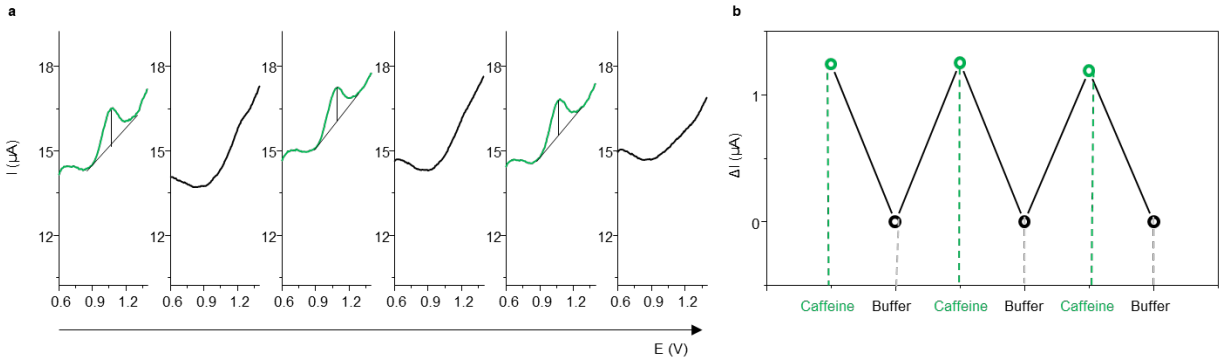

Supplementary Figure 20. Reversibility test for the voltammetric caffeine sensor. Solutions containing only acetate buffer 0.01M, pH 4.5 and 200 µM of caffeine in the same buffer were measured alternately. **a**, DPV for caffeine (green) followed by the DPV of the acetate buffer. Every time the solution was wiped from the electrode surface, and surface rinsed with buffer for the next measurement of buffer or caffeine. **b**, Peak current for each caffeine measurement compared with the buffer alone; the buffer signal was normalized to zero.

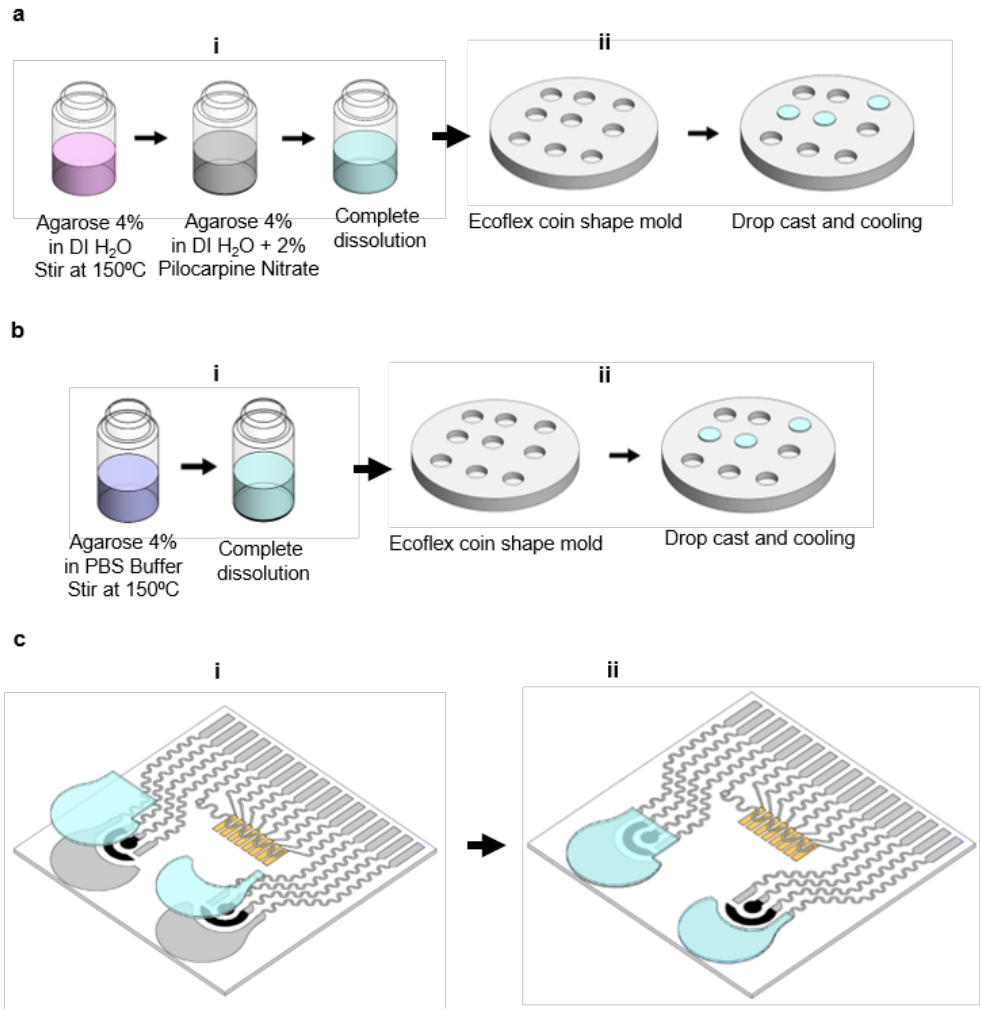

Supplementary Figure 21. Preparation and assembling of the hydrogel layers. **a**, Anode hydrogel preparation. (i) A mixture of 4% agarose and DI water kept under continuous stirring at 150ºC until complete dissolution. Next, the addition of 2% pilocarpine nitrate under stirring. (ii) 300 µL of the solution was then drop cast in the Ecoflex molds. After cooling, the viscous solution on the mold became a solid coin shape hydrogel. **b,** Cathode hydrogel preparation: (i) The mixture of 4% agarose and 0.1 M PBS (pH 7.4) buffer was kept at continuous stirring at 150ºC until observing complete agarose dissolution. (ii) 300 µL of the solution was then drop cast in Ecoflex molds. After cooling, the viscous solution on the mold became a solid coin shape hydrogel. **c,** Hydrogel assembly: (i) A coin shape anode and cathode hydrogel disks were cut with the shape of the screen-printed pattern of the anode and cathode respectively. (ii) After the shape was provided, the anode hydrogel was placed on the left side and the cathode hydrogel was placed on the right side.

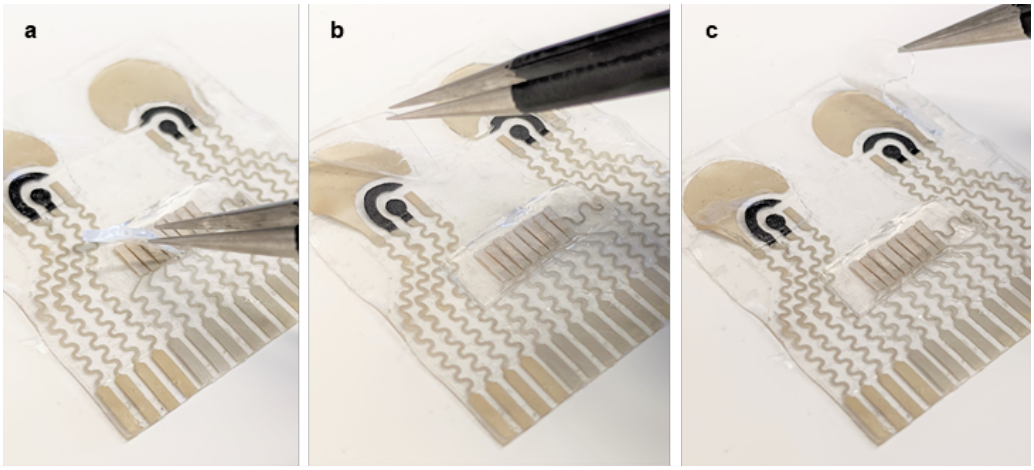

Supplementary Figure 22. Assembly of the iontophoretic and US hydrogels. **a,** The commercial solid gel pad for ultrasound inspection integrated on the device. The picture shows a freestanding cut piece of solid gel. The hydrogels for cathode and anode were cut into the shape of the IP electrodes. **b,** After the shape was provided, **c,** the anode hydrogel was placed on the left side and the cathode hydrogel was placed on the right side.

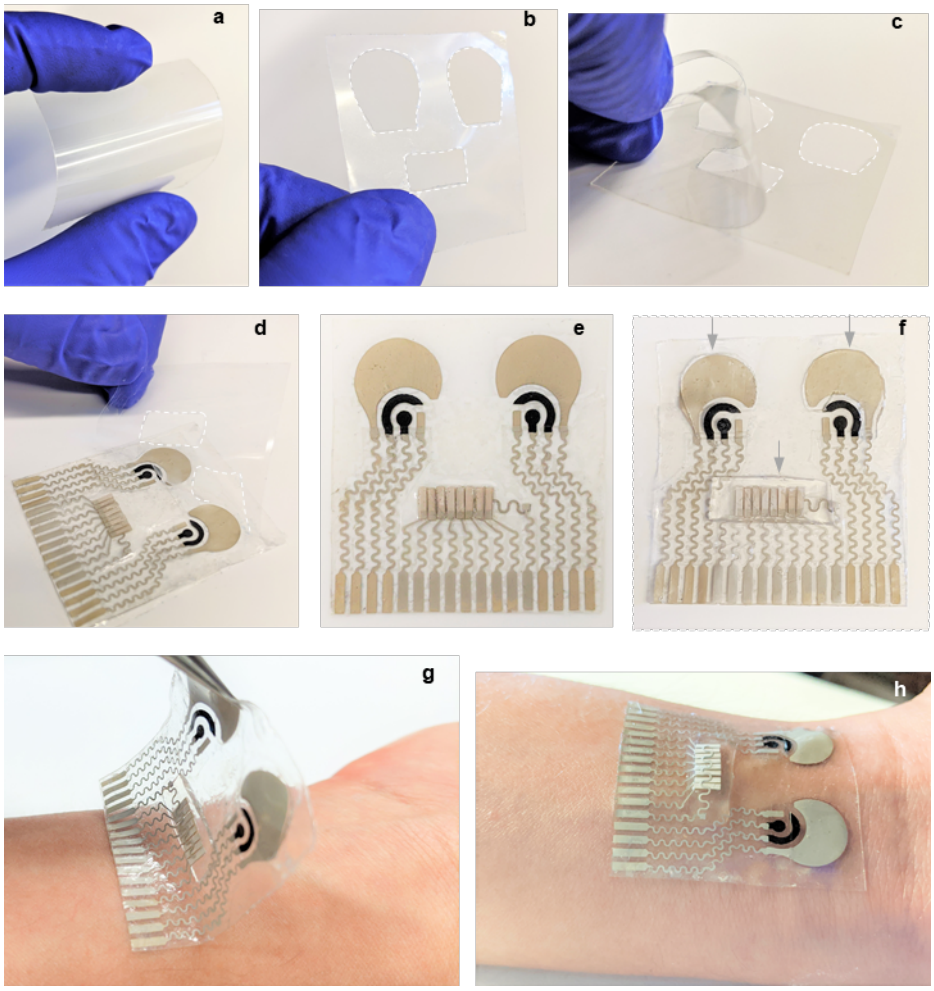

Supplementary Figure 23. Transfer process of the patch. **a,** Double-sided tattoo adhesive. **b,** Opening for the sensing areas, **c,** removing the first protective layer from the double-sided tattoo adhesive with an opening for the sensing areas, and **d,** applying adhesive to the tattoo; **e,** after removing the second protective layer from the applied adhesive, **f,** placing the hydrogels and US gel and **g-h,** transferring to the body.

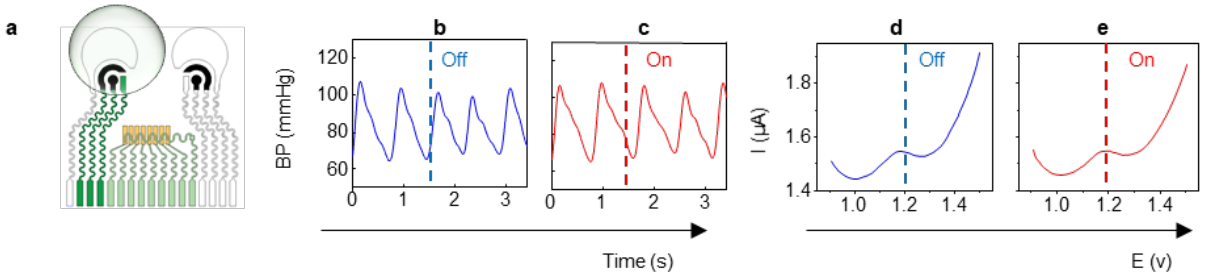

Supplementary Figure 24. Characterization of multimodal wearable sensors. **a,** Signal interference study between the sweat caffeine electrochemical sensor (left side) and the BP transducer, including **b,** BP signal recording while initially sweeping the potential for caffeine detection followed by terminating the sweeping (off), and **c,** BP signal recording while the potential sweeping for caffeine detection is off followed by initiating the sweeping (on). The effect of the BP signal on the caffeine detection was also investigated. **d,** DPV was recording for caffeine detection while the BP was active, following by terminating the BP signal acquisition (off), and **e,** DPV recording for caffeine detection while the BP was inactive, following by initiating the BP signal acquisition (on).

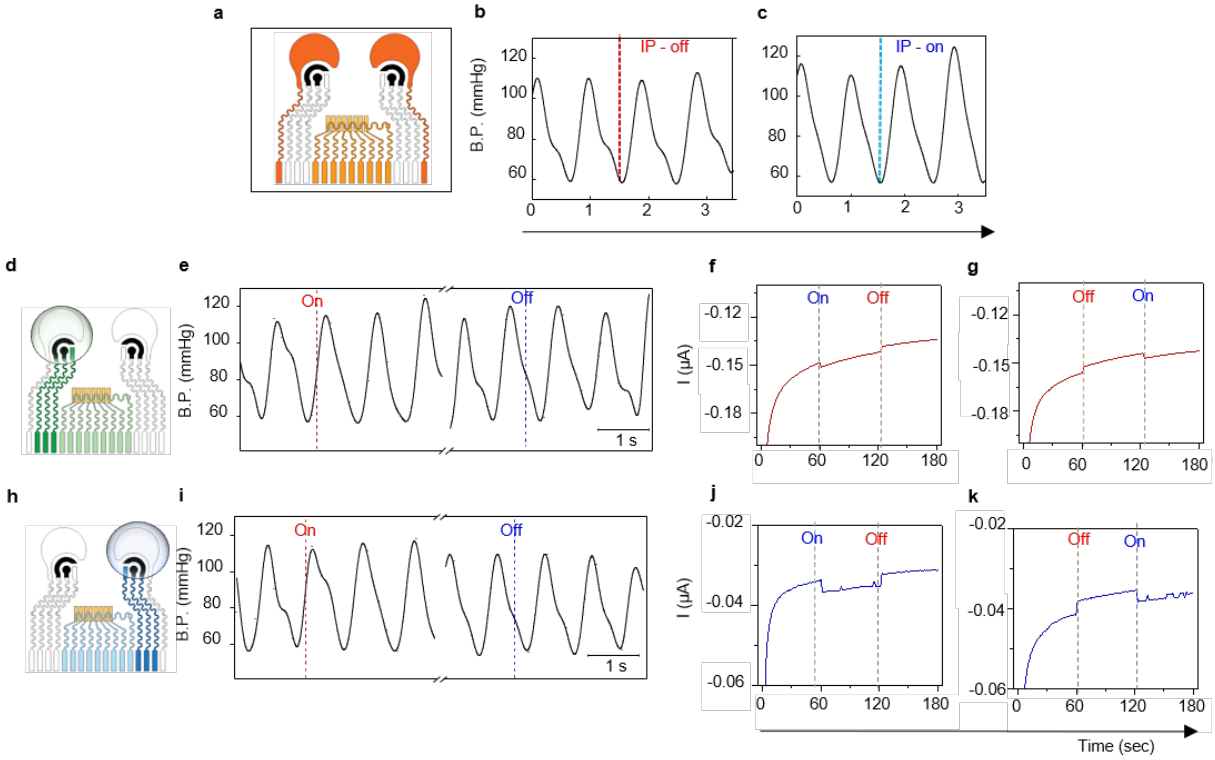

Supplementary Figure 25. On-body cross-talking evaluation of multimodal wearable sensor. a, Signal interference study between iontophoretic current (0.3 mA/cm^2) applied between cathode and anode (dark orange color) and blood pressure device (light orange color). **b**, Blood pressure waveform recorded when the IP current was initially on, and next turned off. **c**, Blood pressure waveform recorded when the IP current was initially off and then turned on. **d**, Cross talking study between detection potential for glucose (dark green) and the blood pressure ultrasound device (light green). **e,** BP signal recorded while the detection potential was initially off, followed by turning the detection potential (-0.2V) on (red dotted line) and off (blue dotted line). **f-g,** Glucose signal recording while applying an on/off ultrasound cycle every 60 seconds for 3 min. **h**, Cross talking study between the lactate detection (dark blue) and the blood pressure ultrasound device (light blue). **i**, BP signal recorded while the detection potential was initially off, followed by turning the detection potential -0.2V on (red dotted line) and off (blue dotted line). **j**, Lactate signal recording while applying the ultrasound cycle on/off every 60 seconds for 3 min. **k,** Lactate signal recording while applying the ultrasound cycle off/on every 60 seconds for 3 min.

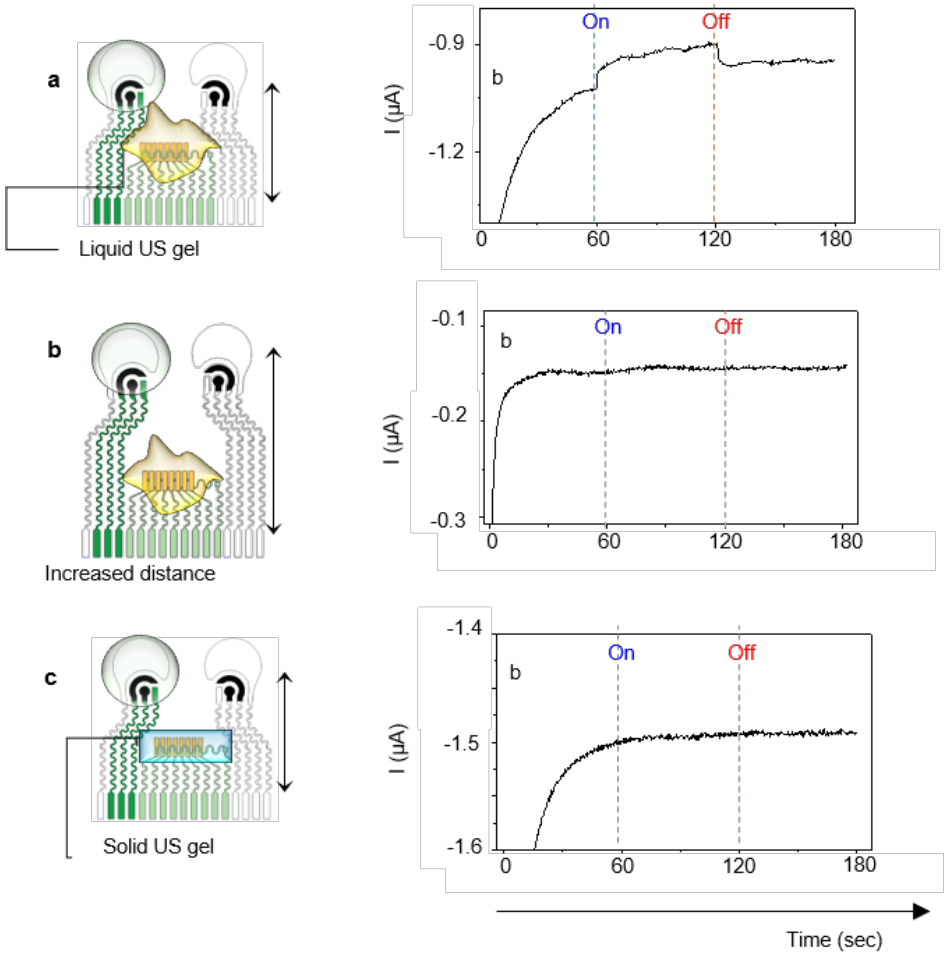

Supplementary Figure 26. In-vitro cross-talking evaluation of multimodal wearable sensor. In vitro measurements were performed using the agarose-PBS hydrogel and the ultrasound gel placed over the blood pressure transducers. **a,** The PBS hydrogel and ultrasound gel were in contact while the ultrasound pulse was turned on and off (right), respectively. A decreasing (more positive current) was observed when the gels were in contact. **b**, A different design with increased distance between the gels were used in vitro with the same amount of ultrasound gel, due to the physical distance, no cross-talking was observed (right). **c**, The same design (with a shorter distance between the blood pressure and chemical sensors) was used with a solid hydrogel and no apparent cross-talking was observed (right).

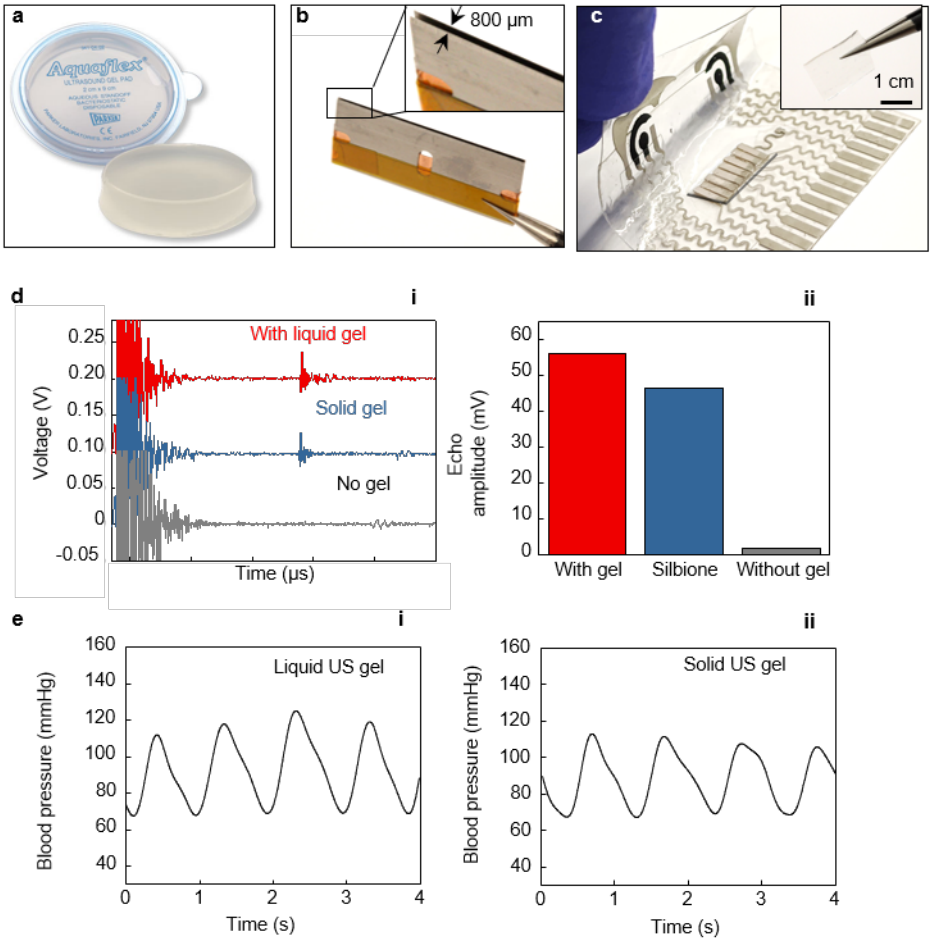

Supplementary Figure 27. Preparation and test of solid ultrasound gel. a, The commercial solid gel pad for ultrasound inspection. **b,** The razor blades used to cut a thin slice of solid ultrasound gel; the insert shows the gap between the blades is 800 µm. **c**, Integrated solid gel on the device. The insert shows a freestanding cut piece of solid gel. **d**, Ultrasound penetration intensity test with a pulse-echo test is performed in (i) using a phantom Ecoflex with the liquid and solid ultrasound gel and in the absence of the gel. The respective echo amplitude is compared in (ii). **e,** On-body experiment comparing the BP waveform measured with (i) liquid and (ii) solid ultrasound gel.

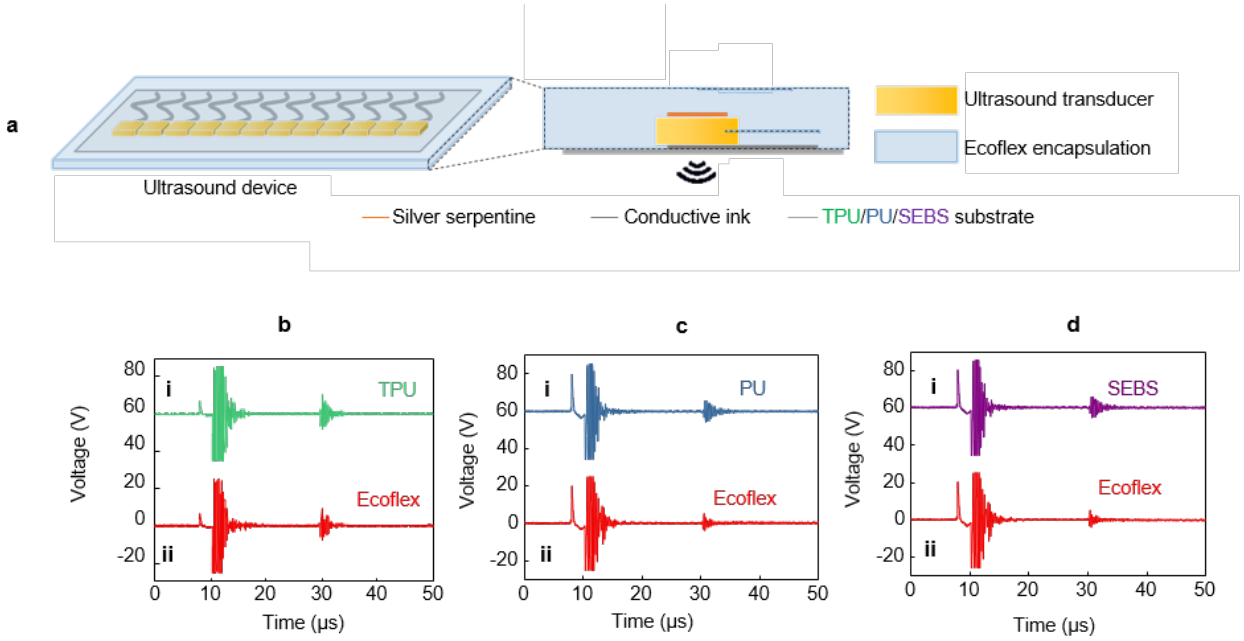

Supplementary Figure 28. Effect of substrate on the ultrasound transmission. The substrates with certain ultrasound impedance will result in a different ultrasound penetration intensity. **a,** Illustration of the fabrication process. A pulse-echo test is performed on different materials as substrates, including **b-i,** TPU, **c-i,** PU, **d-i,** SEBS, and (ii) Ecoflex. The echo signal intensity is directly compared to the ultrasound penetration.

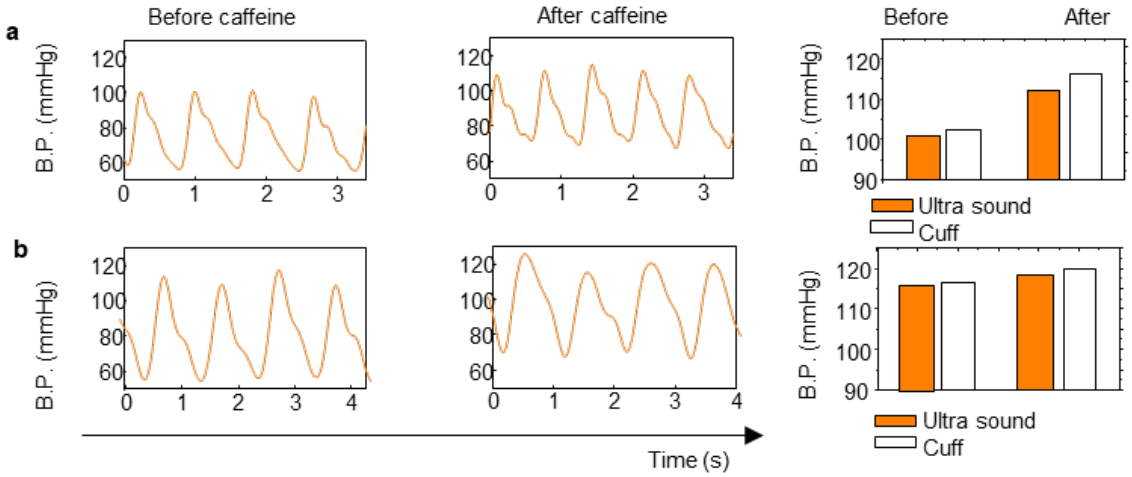

Supplementary Figure 29. On body evaluation for caffeine intake. a, On-body evaluation of BP changes for a volunteer with no habitual caffeine intake (caffeine intolerant)**.** Before and after caffeine sugar-free beverage consumption (Right). Bar graphics represent the sensor validation using a commercial cuff (white) and BP readings obtained with the ultrasound transducers (orange). **b,** On-body evaluation of BP changes for a volunteer with regular caffeine intake habits (caffeine tolerant)**.** Before and after caffeine sugar-free beverage consumption (Right). Bar graphics represent the sensor validation using a commercial cuff (white) and BP readings obtained with the ultrasound transducers (orange).

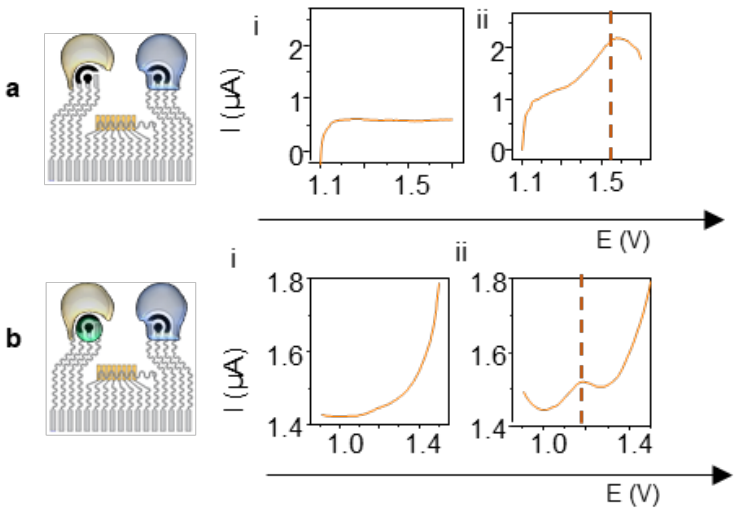

Supplementary Figure 30. On-body caffeine detection and pH variation. a, Schematic showing gel configuration for caffeine detection in stimulated sweat without the use of acetate buffer over the caffeine sensor. The baseline before caffeine intake presents no peak (i), while the caffeine peak is presented at 1.6V when the caffeine sensor is in direct contact with sweat (~pH 7). b, Schematic showing the gel configuration using an acetate buffer pH 4.5 loaded agarose gel on the caffeine sensor (green gel). The baseline before caffeine intake presents no peak (i), while a defined caffeine peak is presented at 1.2V when the caffeine sensor is in contact with the acetate buffer gel (ii).

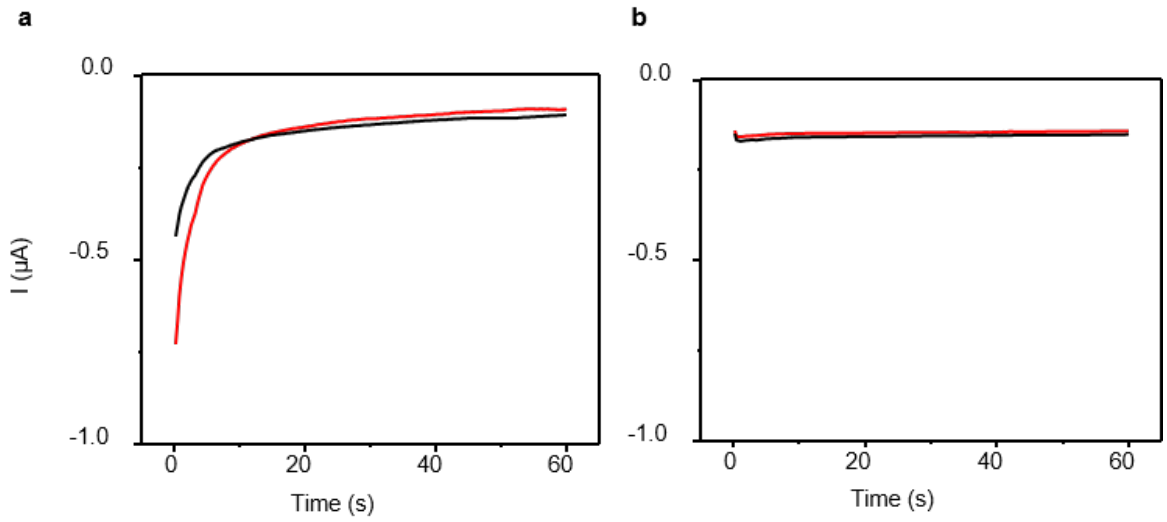

Supplementary Figure 31. Control experiment: Electrochemical sensors without the sensing recognition layer. a, Cathode sensor signal recorded after the first ISF extraction (red line) and after the second ISF extraction (black line). **b**, Anode sensor signal recorded in the first sweat stimulation (red line) and during the second sweat stimulation (black line). Applied potential, -0.2 V.

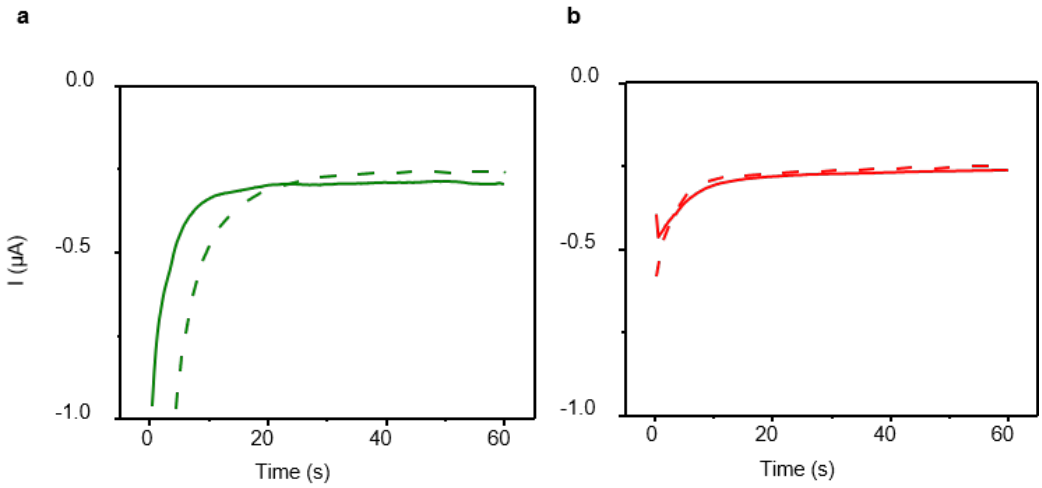

Supplementary Figure 32. Control experiments: Response for lactate and glucose recording without exercise and food ingestion. a, The lactate sensor response after the first sweat stimulation (green dash line) and second sweat stimulation (green solid line). **b**, The glucose sensor response after the first ISF extraction (red dash line) and second ISF extraction (red solid line). Applied potential, -0.2 V.

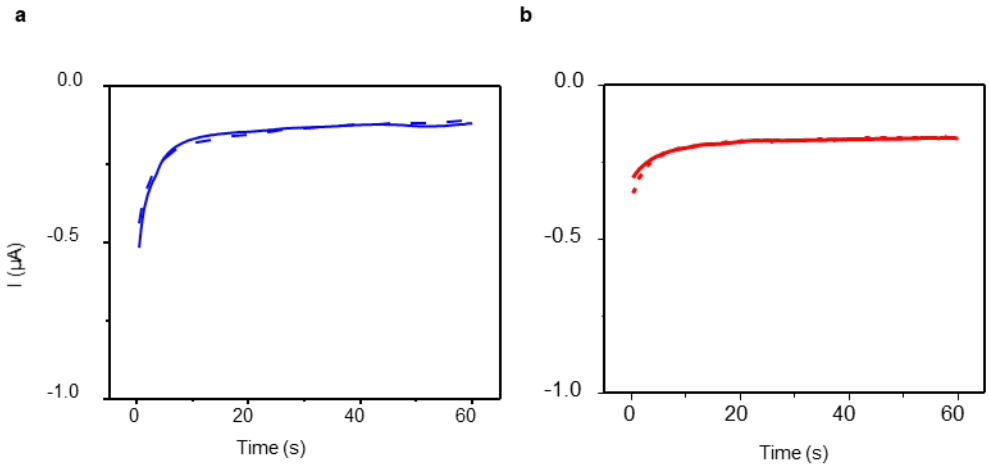

Supplementary Figure 33. Control experiments: Response for alcohol and glucose recording without alcohol and food ingestion. a, The alcohol the first sweat stimulation (blue dash line) and second sweat stimulation (blue solid line). **b**, Response of the glucose sensor after the first ISF extraction (red dash line) and second ISF extraction (red solid line). Applied potential, -0.2 V.

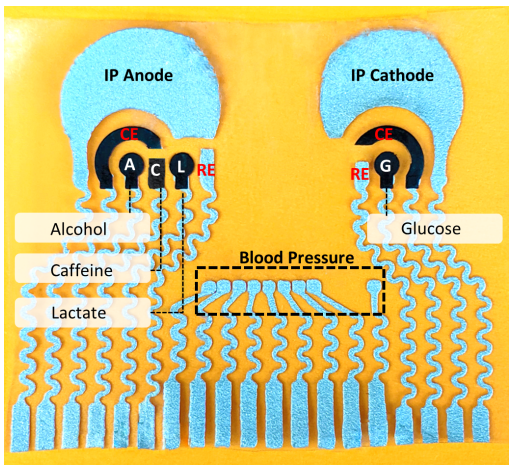

Supplementary Figure 34. Design of an epidermal patch for the simultaneous monitoring of blood pressure along with sweat alcohol, caffeine and lactate, and ISF glucose chemical markers.

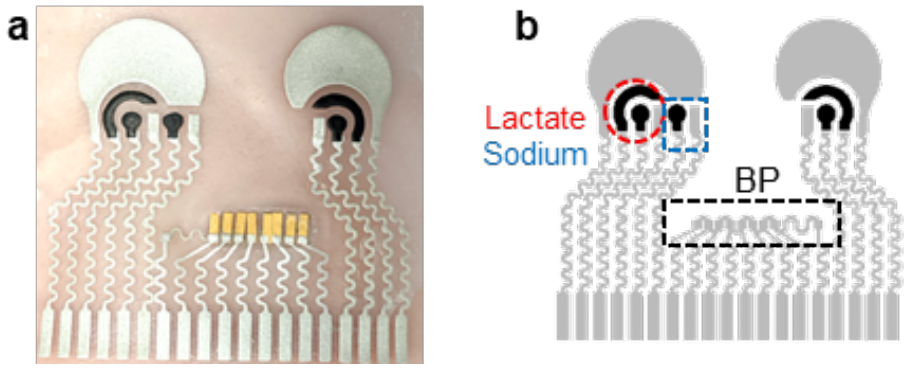

Supplementary Figure 35. Design of the stretchable integrated blood pressure-chemical sensing patch for the simultaneous detection of sweat sodium and lactate, and blood pressure. **a**, A photo image of the sensor on the body. **b**, Illustration of the sensor's acoustic and electrochemical sensing components. Lactate and sodium sensors are located at the cathodic compartment. A three-electrodes system is used for lactate detection (red circle) and a two-electrode system is used for sodium detection (blue square). The blood pressure sensor is located in the center on the patch (black square).

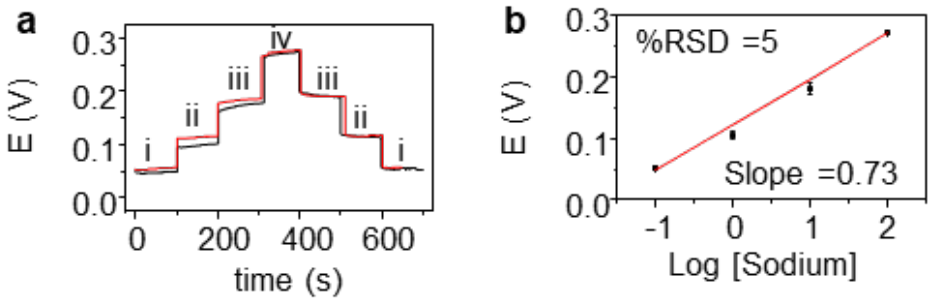

Supplementary Figure 36. In vitro characterization of the sodium sensor. a, Reversibility test for the sequential increasing and decreasing NaCl concentrations in a single sensor. The reversibility was realized for two sensors (red and black curves) using **i**, 0.1 mM, **ii**, 1 mM, **iii**, 10 mM and **iv**, 100 mM of NaCl. **b,** Calibration curve for the response of the sodium sensor to concentrations i-iv. (n=5, RSD=5%, Slope =0.73, r^2=0.99).

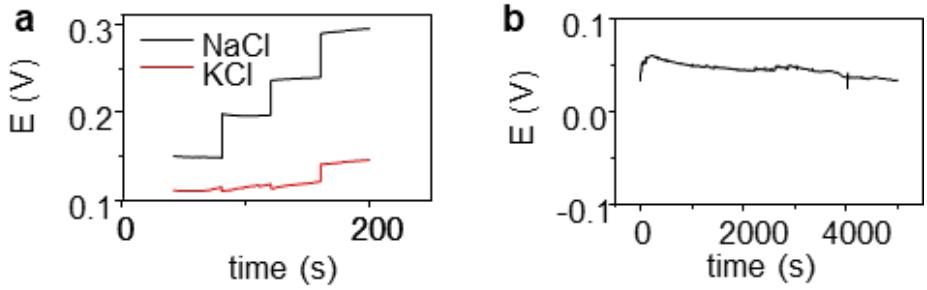

Supplementary Figure 37. In vitro characterization of the sodium sensor. a, Interference test comparing the potentiometric sensor response to NaCl vs KCl, using increasing concentrations of 0.1, 1, 10, and 100 mM of NaCl (black curve) and KCL (red curve). **b,** Stability of the sodium potentiometric response during a continuous 75 min monitoring of 0.1 mM NaCl.

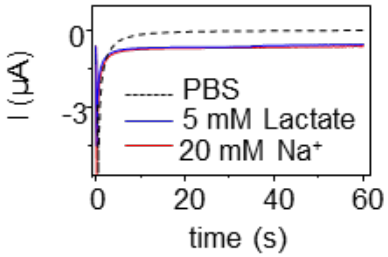

Supplementary Figure 38. In vitro characterization of the lactate sensor in the presence of sodium. Effect of sodium upon the amperometric response of the lactate sensor. A stable PBS baseline was acquired at -0.2V (dotted line) followed by the addition of 5 mM lactate (blue curve), and subsequent addition of 20 mM NaCl (red curve).

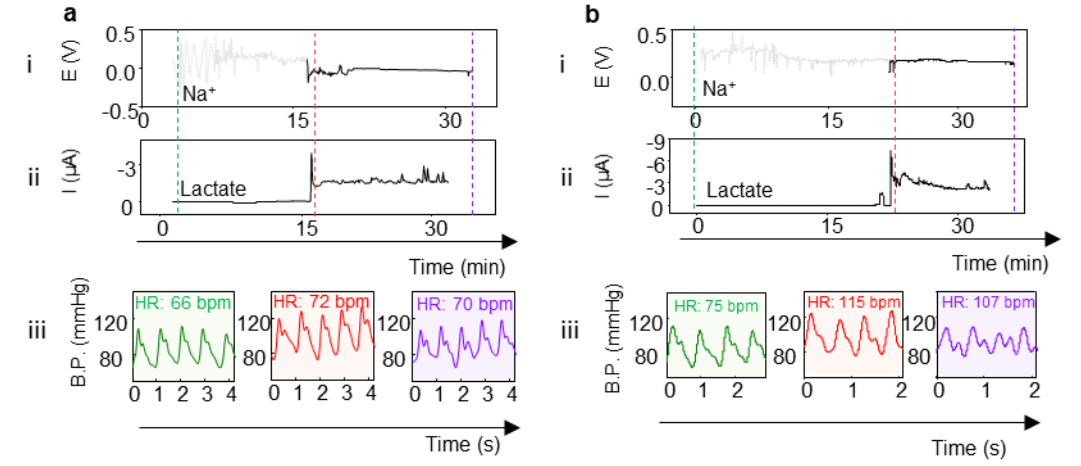

Supplementary Figure 39. Continuous Sodium/lactate//BP/HR performance. **a**, Continuous signal recording showing sweat sodium (i) and lactate (i) profile during stationary biking for fit subject. BP/HR signal recording before (green), during (red), and after (purple) stationary biking (iii). **b**, Continuous signal recording showing sweat sodium (i) and lactate (i) profile during stationary biking for a sedentary subject. BP/HR signal recording before (green), during (red), and after (purple) stationary biking (iii).

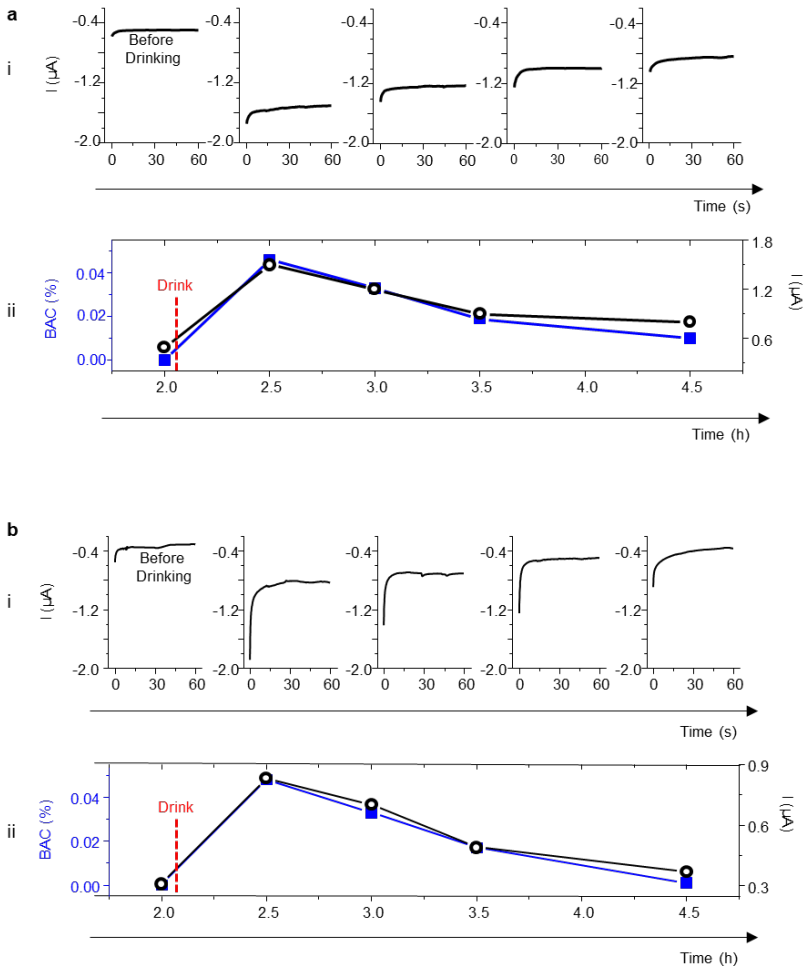

Supplementary Figure 40. Continuous Alcohol monitoring in stimulated sweat for two volunteers. a, b Continuous alcohol monitoring was performed by measuring alcohol levels in sweat every 10 minutes. Sweat was stimulated before drinking alcohol by performing 10 minutes IP, followed by 5 minutes waiting time for sweat generation. Chronoamperometry was performed and the fifth amperogram was taken (i). Therefore, the total time for the final signal was 30 minutes. After every sweat stimulation a breathalyzer was used to measure BAC. Sweat was stimulated every 10 minutes until ~ zero BAC, and the correlation between sweat alcohol (black plot) and blood alcohol (blue plot) is shown in the bottom plot (ii).

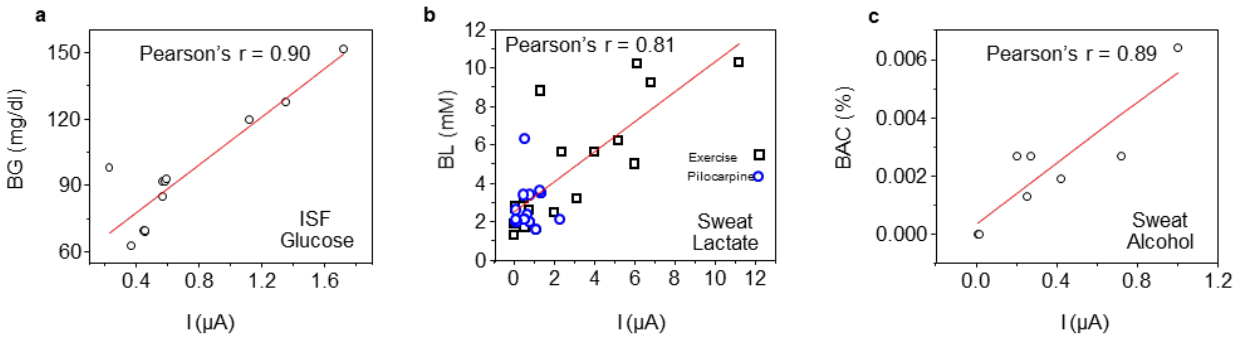

Supplementary Figure 41. Correlation curves for sweat and ISF analytes. **a**, Correlation curve for ISF glucose and blood glucose (n = 13). **b**, Correlation curve for sweat lactate and blood lactate = 32 (n=18). **c**, Correlation curve for sweat alcohol and blood alcohol (n = 10).

Supplementary Videos

Video S1. Application of hydrogels on the device

Video S2. Artery movement during cycling